4a). We also evaluated the ratio of colocalization of pDNA and lamp-2. In normal medium, the ratio of colocalization of pDNA and lamp-2 was decreased by the application of BLs and US. By contrast, the decrease in the ratio of colocalization of pDNA and lamp-2 could be abrogated by 10 mM EGTA and ATP depletion (Figure 4b). These results suggest that BLs and US exposure could decrease the ratio of colocalization of pDNA and lysosomes. Furthermore, Ca^{2+} and ATP may be involved in the escape of AG73-PEG liposomes from lysosomes. We also confirmed the change of localization of pDNA with endosomes or lysosomes. When 293T-Syn2 cells were treated by AG73-PEG liposomes with BLs and US exposure, a decrease in colocalization of pDNA and endosomes was observed at 10 min after US exposure,[9] whereas a decrease in colocalization of pDNA and lysosomes was observed at 60 min after US exposure (Figure 3). These results suggest that BLs and US exposure might significantly affect endosomes, leading to the decrease in colocalization of pDNA and endosomes. In addition, the increase in the release of genes to the cytosol from endosomes might decrease gene delivery from endosomes to lysosomes.

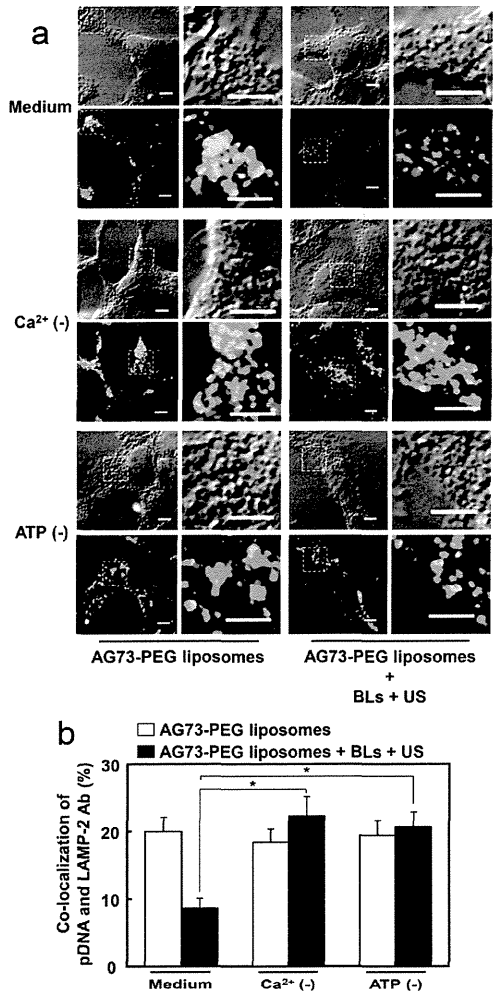

Figure 4. Effects of Ca^{2+} and ATP on intracellular localization of pDNA and lysosome. (a, b) The 293T-Syn2 cells were treated with AG73-PEG liposomes encapsulating Cy3-labeled pDNA (red) for 4 h at 37 °C and then washed twice with Ca^{2+}-free DMEM containing 10 mM EGTA to create Ca^{2+}-depleted conditions. ATP was depleted by pretreating cells for 30 min before US exposure with 1 μg/mL antimycin A, 10 mM NaF, and 0.1% NaN_3. BLs (120 μg/mL) were added to cells followed by immediate US exposure. The cells were incubated for 1 h, fixed with 4% paraformaldehyde for 1 h at 4 °C and stained with antibodies for lamp-2 (green), a marker for lysosomes. The cells were observed by CLSM. The areas within the dotted square are shown as enlarged images. The scale bars represent 5 μm. The ratio of colocalization of Cy3-labeled pDNA with lamp-2 was quantified. The data are shown as means ± SE (n = 50). *p < 0.05 (Mann–Whitney's U test).

On the other hand, it has been also reported that US exposure could affect the transcription by oxidative stress or activation of NFκB.[35,36] It may be possible that an activated transcription is involved in enhanced gene transfection. We need more study to clarify the detailed mechanism concerning transcription in the enhanced gene delivery by BLs and US exposure. However, the endosomal escape of AG73-PEG liposomes induced by BLs and US exposure was significantly suppressed in Ca^{2+} or ATP-depleted condition (Figure 3). Therefore, our results suggest that BLs and US exposure can enhance at least the endosomal escape followed by gene expression via Ca^{2+} and ATP.

Although Ca^{2+} and ATP were involved in enhanced endosomal escape and gene expression efficiency of AG73-PEG liposomes by BLs and US exposure, how Ca^{2+} and ATP enhance the endosomal escape of carriers is still unclear. More investigations into the detailed mechanism of enhanced endosomal escape of AG73-PEG liposomes by BLs and US exposure are required. Moreover, endosomal acidification is adjusted by Ca^{2+}, suggesting that the influx of Ca^{2+} by BL and US exposure may affect endosomal acidification.[26] This could lead to the destabilization of endosomes and hydrogen pumps, such as H^+/K^+-ATPase. However, Ca^{2+} and ATP are involved in endosomal membrane fusion.[27,28] Therefore, an influx of Ca^{2+} by BLs and US exposure and ATP may affect endosomal membrane fusion. Our study demonstrated the involvement of Ca^{2+} and ATP in enhanced endosomal escape and gene expression efficiency of AG73-PEG liposomes by BLs and US exposure. Significantly, BLs and US exposure enhanced endosomal escape through biological effects rather than physical effects. In fact, our results suggest that BLs and US exposure could affect more endosomes than lysosomes. It is expected that BLs and US exposure could be safer tools for the enhancement of endosomal escape by setting the appropriate US exposure conditions.

In conclusion, our study focused on Ca^{2+} and ATP and investigated the particular mechanism of enhanced endosomal escape and gene expression of AG73-PEG liposomes by BLs and US exposure. When cells were treated in Ca^{2+}- and ATP-depleted conditions, endosomal escape and gene expression of AG73-PEG liposomes were not enhanced by BLs and US exposure. These results suggest that both Ca^{2+} and ATP are necessary for enhanced endosomal escape and gene expression of AG73-PEG liposomes by BLs and US exposure. These findings may contribute to the development of useful gene transfection methods to achieve efficient gene transfection by improving endosomal escape.

■ AUTHOR INFORMATION

Corresponding Author

*Tokyo University of Pharmacy and Life Sciences, School of Pharmacy, Drug and Gene Delivery Systems, 1432-1

Horinouchi, Hachioji, Tokyo 192-0392, Japan. Tel and fax: +81-42-676-3183. E-mail: negishi@toyaku.ac.jp.

Notes

The authors declare no competing financial interest.

■ ACKNOWLEDGMENTS

We are grateful to Dr. Katsuro Tachibana (Department of Anatomy, School of Medicine, Fukuoka University) for technical advice regarding the induction of cavitation with US, and to Yasuhiko Hayakawa and Kosho Suzuki (NEPAGENE Co., LTD.) for technical advice regarding exposure to US. This study was supported by an Industrial Technology Research Grant (04A05010) from the New Energy and Industrial Technology Development Organization (NEDO) of Japan, a Grant-in-aid for Exploratory Research (18650146) and a Grant-in-aid for Scientific Research (B) (20300179) from the Japan Society for the Promotion of Science, and by a grant for private universities provided by the Promotion and Mutual Aid Corporation for Private Schools of Japan.

■ ABBREVIATIONS USED

BLs, Bubble liposomes; CLSM, confocal laser scanning microscopy; DOPE, 1,2-dioleoyl-*sn*-glycero-3-phosphoethanolamine; DOPG, 1,2-dioleoyl-*sn*-glycero-3-phospho-*rac*-1-glycerol; DSPE, 1,2-distearoyl-*sn*-glycero-3-phosphatidylethanolamine; FBS, fetal bovine serum; Fmoc, fluorenylmethoxycarbonyl; Mal, maleimide; pDNA, plasmid DNA; PEG, polyethylene glycol; US, ultrasound

■ REFERENCES

(1) Zhang, S.; Xu, Y.; Wang, B.; Qiao, W.; Liu, D.; Li, Z. Cationic compounds used in lipoplexes and polyplexes for gene delivery. *J. Controlled Release* **2004**, *100*, 165–180.

(2) Hama, S.; Akita, H.; Ito, R.; Mizuguchi, H.; Hayakawa, T.; Harashima, H. Quantitative comparison of intracellular trafficking and nuclear transcription between adenoviral and lipoplex systems. *Mol. Ther.* **2006**, *13*, 786–794.

(3) Varga, C. M.; Tedford, N. C.; Thomas, M.; Klibanov, A. M.; Griffith, L. G.; Auffenburger, D. A. Quantitative comparison of polyethylenimine formulations and adenoviral vectors in terms of intracellular gene delivery processes. *Gene Ther.* **2005**, *12*, 1023–1032.

(4) Hatakeyama, H.; Ito, E.; Akita, H.; Oishi, M.; Nagasaki, Y.; Futaki, S.; Harashima, H. A pH-sensitive fusogenic peptide facilitates endosomal escape and greatly enhances the gene silencing of siRNA-containing nanoparticles in vitro and in vivo. *J. Controlled Release* **2009**, *139*, 127–132.

(5) Subbarao, N. K.; Parente, R. A.; Szoka, F. C.; Nadasdi, L.; Pongracz, K. pH-dependent bilayer destabilization by an amphipathic peptide. *Biochemistry* **1987**, *26*, 2964–2972.

(6) Lee, S. H.; Choi, S. H.; Kim, S. H.; Park, T. G. Thermally sensitive cationic polymer nanocapsules for specific cytosolic delivery and efficient gene silencing of siRNA: swelling induced physical disruption of endosome by cold shock. *J. Controlled Release* **2008**, *125*, 25–32.

(7) Høgset, A.; Prasmickaite, L.; Selbo, P. K.; Hellum, M.; Engesaeter, B. Ø.; Bonsted, A.; Berg, K. Photochemical internalisation in drug and gene delivery. *Adv. Drug Delivery Rev.* **2004**, *56*, 95–115.

(8) Negishi, Y.; Omata, D.; Iijima, H.; Hamano, N.; Endo-Takahashi, Y.; Nomizu, M.; Aramaki, Y. Preparation and characterization of laminin-derived peptide AG73-coated liposomes as a selective gene delivery tool. *Biol. Pharm. Bull.* **2010**, *33*, 1766–1769.

(9) Negishi, Y.; Omata, D.; Iijima, H.; Takabayashi, Y.; Suzuki, K.; Endo, Y.; Suzuki, R.; Maruyama, K.; Nomizu, M.; Aramaki, Y. Enhanced laminin-derived peptide AG73-mediated liposomal gene transfer by bubble liposomes and ultrasound. *Mol. Pharmaceutics* **2010**, *7*, 217–226.

(10) Omata, D.; Negishi, Y.; Hagiwara, S.; Yamamura, S.; Endo-Takahashi, Y.; Suzuki, R.; Maruyama, K.; Nomizu, M.; Aramaki, Y. Bubble liposomes and ultrasound promoted endosomal escape of TAT-PEG liposomes as gene delivery carriers. *Mol. Pharmaceutics* **2011**, *8* (6), 2416–2423.

(11) Delius, M.; Adams, G. Shock wave permeabilization with ribosome inactivating proteins; a new approach to tumor therapy. *Cancer Res.* **1999**, *59*, 5227–5232.

(12) Taniyam, Y.; Tachibana, K.; Hiraoka, K.; Aoki, M.; Yamamoto, S.; Matsumoto, K.; Nakamura, T.; Ogihara, T.; Kaneda, Y.; Morishita, R. Development of safe and efficient novel nonviral gene transfer using ultrasound: enhancement of transfection efficiency of naked plasmid DNA in skeletal muscle. *Gene Ther.* **2002**, *9*, 260–269.

(13) Negishi, Y.; Matsuo, K.; Endo-Takahashi, Y.; Suzuki, K.; Matsuki, Y.; Takagi, N.; Suzuki, R.; Maruyama, K.; Aramaki, Y. Delivery of an angiogenic gene into ischemic muscle by novel bubble liposomes followed by ultrasound exposure. *Pharm. Res.* **2011**, *28*, 712–719.

(14) Negishi, Y.; Endo, Y.; Fukuyama, T.; Suzuki, R.; Takizawa, T.; Omata, D.; Maruyama, K.; Aramaki, Y. Delivery of siRNA into the cytoplasm by liposomal bubbles and ultrasound. *J. Controlled Release* **2008**, *132*, 124–130.

(15) Negishi, Y.; Endo-Takahashi, Y.; Ishii, K.; Suzuki, R.; Oguri, Y.; Murakami, T.; Maruyama, K.; Aramaki, Y. Development of novel nucleic acid-loaded bubble liposomes using cholesterol-conjugated siRNA. *J. Drug Targeting* **2011**, *19*, 830–836.

(16) Suzuki, R.; Namai, E.; Oda, Y.; Nishiie, N.; Otake, S.; Koshima, R.; Hirata, K.; Taira, Y.; Utoguchi, N.; Negishi, Y.; Nakagawa, S.; Maruyama, K. Cancer gene therapy by IL-12 gene delivery using liposomal bubbles and tumoral ultrasound exposure. *J. Controlled Release* **2010**, *142*, 245–250.

(17) Warden, S. J.; Fuchs, R. K.; Kessler, C. K.; Avin, K. G.; Cardinal, R. E.; Stewart, R. L. Ultrasound produced by a conventional therapeutic ultrasound unit accelerates fracture repair. *Phys. Ther.* **2006**, *86*, 1118–1127.

(18) Warden, S. J. A new direction for ultrasound therapy in sports medicine. *Sports Med.* **2003**, *33*, 95–107.

(19) Feril, L. B. Jr.; Kondo, T.; Zhac, Q. L.; Ogawa, R.; Tachibana, K.; Kudo, N.; Fujimoto, S.; Nakamura, S. Enhancement of ultrasound-induced apoptosis and cell lysis by echo-contrast agents. *Ultrasound Med. Biol.* **2003**, *29*, 331–337.

(20) Juffermans, L. J.; Dijkmans, P. A.; Musters, R. J.; Visser, C. A.; Kamp, O. Transient permeabilization of cell membranes by ultrasound-exposed microbubbles is related to formation of hydrogen peroxide. *Am. J. Physiol.* **2006**, *291*, H1595–H1601.

(21) Juffermans, L. J.; Kamp, O.; Dijkmans, P. A.; Visser, C. A.; Musters, R. J. Low-intensity ultrasound-exposed microbubbles provoke local hyperpolarization of the cell membrane via activation of BK(Ca) channels. *Ultrasound Med. Biol.* **2008**, *34*, 502–508.

(22) Zhou, Y.; Shi, J.; Cui, J.; Deng, C. X. Effects of extracellular calcium on cell membrane resealing in sonoporation. *J. Controlled Release* **2008**, *126*, 34–43.

(23) Takeuchi, R.; Ryo, A.; Komitsu, N.; Mikuni-Takagaki, Y.; Fukui, A.; Takagi, Y.; Shiraishi, T.; Morishita, S.; Yamazaki, Y.; Kumagai, K.; Aoki, I.; Saito, T. Low-intensity pulsed ultrasound activates the phosphatidylinositol 3 kinase/AKT pathway and stimulates the growth of chondrocytes in three-dimensional cultures: a basic science study. *Arthritis Res. Ther.* **2008**, *10*, R77.

(24) Giacomello, M.; Drago, I.; Pizzo, P.; Pozzan, T. Mitochondrial Ca^{2+} as a key regurator of cell life and death. *Cell Death Differ.* **2007**, *14*, 1267–1274.

(25) Hassan, M. A.; Cambell, P.; Kondo, T. The role of Ca^{2+} in ultrasound-elicited bioeffects: progress, perspective and prospects. *Drug Discovery Today* **2010**, *15*, 892–906.

(26) Lelouvier, B.; Puertollano, R. Mucolipin-3 regulates luminal calcium, acidification, and membrane fusion in the endosomal pathway. *J. Biol. Chem.* **2011**, *286*, 9826–9832.

(27) Yan, Q.; Sun, W.; McNew, J. A.; Vida, T. A.; Bean, A. J. Ca^{2+} and N-ethylmaleimide-sensitive factor differentially regulate disassembly of SNARE complexes on early endosomes. *J. Biol. Chem.* **2004**, *279*, 18270−18276.
(28) Mayorga, L. S.; Berón, W.; Sarrouf, M. N.; Colombo, M. I.; Creutz, C.; Stahl, P. D. Calcium-dependent fusion among endosomes. *J. Biol. Chem.* **1994**, *269*, 30927−30934.
(29) Rescher, U.; Zobiack, N.; Gerke, V. Intact Ca2+-binding sites are required for targeting of annxin 1 to endosomal membranes in living HeLa cells. *J. Cell Sci.* **2000**, *113*, 3931−3938.
(30) Suh, J.; Wirtz, D.; Hanes, J. Efficient active transport of gene nanocarriers to the cell nucleus. *Proc. Natl. Acad. Sci. U.S.A.* **2003**, *100*, 3878−3882.
(31) Oba, M.; Aoyagi, K.; Miyata, K.; Matsumoto, Y.; Itaka, K.; Nishiyama, N.; Yamasaki, Y.; Koyama, H.; Kataoka, K. Polyplex micelles with cyclic RGD peptide ligands and disulfide cross-links directing to the enhanced transfection via controlled intracellular trafficking. *Mol. Pharmaceutics* **2008**, *5*, 1080−1092.
(32) Idone, V.; Tam, C.; Goss, J. W.; Toomre, D.; Pypaert, M.; Andrews, N. W. Repair of injured plasma membrane by rapid Ca^{2+}-dependent endocytosis. *J. Cell Biol.* **2008**, *180*, 905−914.
(33) Rothenberger, S.; Iacopetta, B. J.; Kühn, L. C. Endocytosis of the transferrin receptor requires the cytoplasmic domain but not its phosphorylation site. *Cell* **1987**, *49*, 423−431.
(34) Kannan, K.; Stewart, R. M.; Bounds, W.; Carlsson, S. R.; Fukuda, M.; Betzing, K. W.; Holcombe, R. F. Lysosome-associated membrane proteins h-LAMP1 (CD107a) and h-LAMP2 (CD107b) are activation-dependent cell surface glycoproteins in human peripheral blood mononuclear cells which mediate cell adhesion to vascular endothelium. *Cell Immunol.* **1996**, *171*, 10−19.
(35) Kagiya, G.; Ogawa, R.; Ito, S.; Fukuda, S.; Hatashita, M.; Tanaka, Y.; Yamamoto, K.; Kondo, T. Identification of a cis-acting element responsive to ultrasound in the 5′-flanking region of the human heme oxygenase-1 gene. *Ultrasound Med. Biol.* **2009**, *35*, 155−164.
(36) Un, K.; Kawakami, S.; Higuchi, Y.; Suzuki, R.; Maruyama, K.; Yamashita, F.; Hashida, M. Involvement of activated transcriptional process in efficient gene transfection using unmodified and mannose-modified bubble lipoplexes with ultrasound exposure. *J. Controlled Release* **2011**, *156*, 355−363.

Journal of Controlled Release 160 (2012) 362–366

Contents lists available at SciVerse ScienceDirect

Journal of Controlled Release

journal homepage: www.elsevier.com/locate/jconrel

Prophylactic immunization with Bubble liposomes and ultrasound-treated dendritic cells provided a four-fold decrease in the frequency of melanoma lung metastasis

Yusuke Oda [a,1], Ryo Suzuki [a,1], Shota Otake [a,1], Norihito Nishiie [a], Keiichi Hirata [a], Risa Koshima [a], Tetsuya Nomura [a], Naoki Utoguchi [a], Nobuki Kudo [b], Katsuro Tachibana [c], Kazuo Maruyama [a,*]

[a] Department of Biopharmaceutics, School of Pharmaceutical Sciences, Teikyo University, Japan
[b] Laboratory of Biomedical Engineering, Graduate School of Information Science and Technology, Hokkaido University, Japan
[c] Department of Anatomy, School of Medicine, Fukuoka University, Japan

ARTICLE INFO

Article history:
Received 15 July 2011
Accepted 6 December 2011
Available online 13 December 2011

Keywords:
Dendritic cells
Antigen delivery system
Cancer immunotherapy
Ultrasound
Liposomes

ABSTRACT

Melanoma has an early tendency to metastasize, and the majority of the resulting deaths are caused by metastatic melanoma. It is therefore important to develop effective therapies for metastasis. Dendritic cell (DC)-based cancer immunotherapy has been proposed as an effective therapeutic strategy for metastasis and recurrence due to prime tumor-specific cytotoxic T lymphocytes. In this therapy, it is important that DCs present peptides derived from tumor-associated antigens on MHC class I molecules. Previously, we developed an innovative approach capable of directly delivering exogenous antigens into the cytosol of DCs using perfluoropropane gas-entrapping liposomes (Bubble liposomes, BLs) and ultrasound. In the present study, we investigated the prevention of melanoma lung metastasis via DC-based immunotherapy. Specifically, antigens were extracted from melanoma cells and used to treat DCs by BL and ultrasound. Delivery into the DCs by this route did not require the endocytic pathway. The delivery efficiency was approximately 74.1%. DCs treated with melanoma-derived antigens were assessed for *in vivo* efficacy in a mouse model of lung metastasis. Prophylactic immunization with BL/ultrasound-treated DCs provided a four-fold decrease in the frequency of melanoma lung metastases. These *in vitro* and *in vivo* results demonstrate that the combination of BLs and ultrasound is a promising method for antigen delivery system into DCs.

1. Introduction

Melanoma is the most devastating form of skin cancer and represents a leading cause of cancer death. Relative to the tumor mass, melanomas have an early tendency to metastasize; indeed, the majority of melanoma deaths are caused by metastatic disease. As a result, the prognosis for melanoma is poor. In fact, the 5-year survival rate of patients with localized melanoma is up to 90%; in contrast, patients with metastasized melanoma have 5-year survival rates of only 20% [1,2]. Additionally, melanoma is usually resistant to standard chemotherapy, and the response rate for any single agent or combination of agents ranges from 5% to 45% [3,4]. Based on these data, there is a clear need to develop effective therapy for metastasized melanoma. There are various therapeutic methods for metastatic cancer, such as surgical treatment, chemotherapy, radiotherapy, and immunotherapy. Of these methods, immunotherapy may be the most promising because of the possibility of preventing systemic metastasis and recurrence in the long term [5–9].

Dendritic cells (DCs), which are unique antigen-presenting cells capable of priming naive T cells, have been used as vaccine carriers for cancer immunotherapy [6,10]. To induce an effective tumor-specific cytotoxic T-lymphocyte (CTL) response, DCs should abundantly present epitope peptides derived from tumor-associated antigens (TAAs) via major histocompatibility complex (MHC) class I molecules and MHC class II molecules [11]. In general, exogenous antigens (such as TAAs in DCs) are preferentially presented on MHC class II molecules [12,13]. On the other hand, the majority of peptides presented via the MHC class I molecules are generated from endogenously synthesized proteins that are degraded by the proteasome [12]. Therefore, in order to efficiently prime TAA-specific CTLs, it is necessary to develop a novel antigen delivery system that can induce MHC class I-restricted TAA presentation on DCs. Several researchers have studied antigen delivery tools based on the cross-presentation theory of exogenous antigens in DCs [14–19]. Proposed antigen delivery carriers have included liposomes [15,16], poly(γ-glutamic acid) nanoparticles [17], and cholesterol pullulan nanoparticles [18]. All of these carriers deliver the antigens into DCs via the endocytic pathway, inducing the leaking of exogenous antigens from the endosome into the cytosol. Finally, it is thought that the antigens leaked into the cytosol are

Abbreviations: BL, Bubble liposome; CTL, cytotoxic T-lymphocyte; DC, dendritic cell; FITC, fluorescein isothiocyanate; MHC, major histocompatibility complex; MW, molecular weight; PBS, phosphate-buffered saline; TAA, tumor-associated antigen; US, ultrasound.

* Corresponding author at: Department of Biopharmaceutics, School of Pharmaceutical Sciences, Teikyo University, 1091-1 Suwarashi, Midori-ku, Sagamihara, Kanagawa 252-5195, Japan. Tel.: +81 42 685 3722; fax: +81 42 685 3432.
E-mail address: maruyama@pharm.teikyo-u.ac.jp (K. Maruyama).

[1] These authors contributed equally to this work.

0168-3659/$ – see front matter.
doi:10.1016/j.jconrel.2011.12.003

presented on MHC class I molecules. As an alternative, we have sought to use an antigen delivery system that does not rely on the endocytic pathway.

Multiple papers have reported the use of microbubbles for ultrasound-mediated gene and drug delivery [20–26]. In this delivery system, microstreams and microjets, which are induced by disruption of nano/microbubbles exposed to ultrasound, promote the transfer of extracellular materials into cells by opening transient pores in the cell membrane [27,28]. Previously, we described ultrasound-mediated antigen delivery in DCs using Bubble liposomes (BLs) containing perfluoropropane, an ultrasound imaging gas [29]. Using this system, a model antigen (ovalbumin) could be delivered into the cytosol of DCs independent of the endocytic pathway. This technique provided direct entry of the exogenous antigens into the MHC class I presentation pathway, resulting in the priming of exogenous antigen-specific CTLs. We proposed that this system could facilitate the delivery of crude antigens (such as tumor lysates and extracts) because such substrates could enter cells via a transient pore. In the present study, we used fluorescein isothiocyanate (FITC)-dextran as a substrate to characterize antigen delivery by BLs and ultrasound. Additionally, we assessed the possible application of BLs and ultrasound in DC-based immunotherapy in an *in vivo* model of melanoma. Specifically, we delivered tumor-extracted antigens into DCs using BLs and ultrasound, and investigated whether these treated DCs protected mice from lung metastasis.

2. Materials and methods

2.1. Cells

B16/BL6 cells, a C57BL/6-derived melanoma cell line, were cultured in RPMI 1640 (Sigma Co., St. Louis, MO, USA) supplemented with 10% heat inactivated fetal bovine serum (FBS, GIBCO, Invitrogen Co., Carlsbad, CA, USA), 50 U/ml penicillin, and 50 μg/ml streptomycin (Wako Pure Chemical Industries, Osaka, Japan).

2.2. Generation of mouse bone marrow-derived DCs

DCs were generated from bone marrow cells, as described elsewhere [30]. Briefly, bone marrow cells were isolated from C57BL/6 mice and were cultured in RPMI 1640 supplemented with 10% FBS, 50 μM 2-mercaptoethanol (Sigma Co., St. Louis, MO, USA), 50 U/ml penicillin, 50 μg/ml streptomycin, and 40 ng/ml mouse granulocyte-macrophage colony-stimulating factor (GM-CSF, PeproTech Inc., Rocky Hill, NJ, USA). After 8–16 days of culture, non-adherent cells were collected and used as DCs.

2.3. Preparation of BLs

Liposomes composed of 1,2-distearoyl-sn-glycero-phosphatidylcholine (DSPC) (NOF Co., Tokyo, Japan) and 1,2-distearoyl-sn-glycero-3-phosphatidyl-ethanolamine-methoxypolyethyleneglycol (DSPE-PEG (2 k)-OMe (NOF Co.)), 94:6 (mol:mol), were prepared by reverse phase evaporation. BLs were prepared from the liposomes and perfluoropropane (Takachiho Chemical Industrial Co., Ltd., Tokyo, Japan) as reported before [31,32]. Briefly, 5-ml sterilized vials containing 2 ml of the liposome suspension (lipid concentration: 2 mg/ml) were filled with perfluoropropane, capped, and then supercharged with 7.5 ml of perfluoropropane. The vials were placed in a bath-type sonicator (42 kHz, 100 W; BRANSONIC 2510J-DTH, Branson Ultrasonics Co., Danbury, CT, USA) for 5 min to form the BLs. In this method, the liposomes were reconstituted by sonication under the condition of supercharge with perfluoropropane in the 5-ml vial container. At the same time, perfluoropropane would be entrapped within lipids as micelles (composed of DSPC and DSPE-PEG(2k)-OMe), so forming nanobubbles. The lipid nanobubbles were encapsulated within the reconstituted liposomes, the sizes of which were increased from ~150–200 nm to ~500 nm.

2.4. Extraction of antigens from B16/BL6 cells

The extraction of antigens from B16BL/6 cells was performed by a butanol extraction method [33]. B16/BL6 cells were washed twice with phosphate-buffered saline (PBS) and then incubated with PBS containing 2.5% (v/v) 1-butanol. The solution was collected and centrifuged twice at 1600 ×*g* at 4 °C. The supernatant was dialyzed with water using a Spectra/Por Dialysis Membrane (MWCO: 10,000; Spectrum Laboratories, Inc., Rancho Dominguez, CA, USA). The dialysate then was centrifuged at 1600 ×*g* at 4 °C, and the resulting supernatant was freeze-dried.

2.5. FITC-dextran or B16/BL6-extracted antigen delivery following inhibition of the endocytic pathway in DCs

B16/BL6-extracted antigens were labeled with Alexa Fluor 633 Succinimidyl Esters (Invitrogen Co., Carlsbad, CA, USA) (Alexa-B16/BL6). DCs were pretreated with OptiMEM (Invitrogen Co.) containing 10 mM NaN_3 for 1 h at 4 °C to inhibit the endocytic pathway [34,35]. After washing the cells, BLs (120 μg) and FITC-dextran (Sigma Co.) or Alexa-B16/BL6 were added to the DCs in OptiMEM containing 10 mM NaN_3. The DCs were exposed to ultrasound (frequency: 2 MHz, duty: 10%, burst rate: 2.0 Hz, intensity 2.0 W/cm^2, time: 3×10 s (interval: 10 s)) using a Sonopore 4000 (6-mm diameter probe; Nepa Gene Co. Ltd., Chiba, Japan), then washed with PBS containing 10 mM NaN_3. The delivery efficiency of FITC-dextran or Alexa-B16/BL6 delivery was analyzed by flow cytometry [36].

2.6. Immunization with antigen-loaded DCs following BLs and ultrasound

DCs (2.5×10^5 cells) were pulsed with antigens (50 μg) exposed to ultrasound and/or BLs (120 μg) in a 48-well plate; the contents of 10 wells then were collected, pooled, and seeded into 1 well of a 6-well plate. After 1 h of incubation at 37 °C, the DCs were washed with medium and cultured for 24 h at 37 °C. The cells were washed with PBS, and the DCs (1×10^6 cells/100 μl) then were injected intradermally into the backs of C57BL/6 mice twice with a one-week interval.

2.7. B16/BL6 experimental lung metastasis model

C57BL/6 mice were immunized twice with DCs as described above. Seven days after the second immunization, B16/BL6 cells (1×10^5 cells/100 μl) were injected into the tail vein. The mice were sacrificed two weeks after the tumor cell injection, and the lungs were harvested and fixed in neutral buffered formalin (10%). The number of B16/BL6 colonies present on the surface of each set of lungs was determined by visual inspection using a stereoscopic dissecting microscope [37].

2.8. Statistical analysis

Differences in the number of lung metastatic colonies between the experimental groups were compared using non-repeated measures analysis of variance (ANOVA) with post-hoc Dunnett's test.

3. Results

3.1. FITC-dextran delivery into DCs by BLs and ultrasound

In BL/ultrasound antigen delivery, extracellular antigens are delivered into cells via the formation of transient membrane pores. Therefore, this technique is expected to deliver antigens into DCs as a function of both

pore size and molecular substrate size. In the present study, we used various molecular weight (MW) FITC-dextran molecules as model antigens and assessed the delivery efficiency of FITC-dextran into DCs. (Fig. 1(a–c)). In DCs treated with FITC-dextran (MW 4000) alone, the mean fluorescence intensity was 4-fold higher than non-treated DCs (Fig. 1(a)). On the other hand, upon treatment with FITC-dextran, BLs, and ultrasound, the mean fluorescence intensity was 2-fold higher than that with FITC-dextran alone. We also observed similar phenomena upon treatment with other sizes of FITC-dextran (MW 20,000 and 70,000) (Fig. 1(b), (c)). In addition, to assess the effect of molecular size on delivery efficiency, the fluorescence intensity was compared among FITC-dextrans (MW 4000, 20,000 and 70,000) delivered with BLs and ultrasound (Fig. 1(d)). The percentages of FITC-positive cells (M1 gated) were not affected by molecular weight, determined as 86.0% (MW: 4000), 87.3% (MW: 20,000), and 77.4% (MW: 70,000). On the other hand, the fluorescence intensity decreased as the molecular weight increased. The mean of fluorescence intensities were 24.5 (MW: 4000), 22.4 (MW: 20,000), and 16.5 (MW: 70,000).

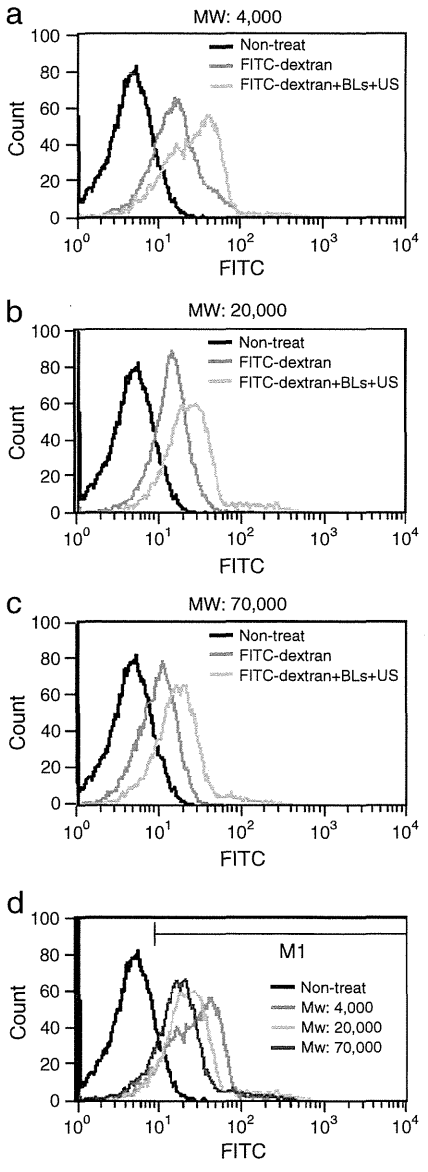

Fig. 1. Effect of molecular size on delivery into DCs using BLs and ultrasound. DCs were incubated with FITC-dextran, exposed to ultrasound in the presence of BLs, and washed with PBS. Delivery efficiency of FITC-dextran was analyzed using flow cytometry. Endocytosis by the DCs was inhibited by the inclusion of 10 mM sodium azide in all solutions and washes. Panels (a) to (c): Experiments were performed with FITC-dextran at a molecular weight of 4000, 20,000, or 70,000, respectively. Panel (d): Molecular weight dependency was analyzed following treatment with the combination of BLs and ultrasound. The percentages of M1 gated cell were quantified as follow: MW: 4000: 86.0%, MW: 20,000: 87.3%, MW: 70,000: 77.4%. The mean of fluorescent intensities were quantified as follow: MW: 4000: 24.5, MW: 20,000: 22.4, MW: 70,000: 16.5.

3.2. B16/BL6-extracted antigen delivery into DCs by BLs and ultrasound

Having demonstrated that the combination of BLs and ultrasound could deliver extracellular molecules of varying sizes, we sought to demonstrate that antigens extracted from B16/BL6 cells could be delivered into DCs by the same technique. Therefore, we assessed the delivery efficiency using Alexa Fluor 633-labeled antigens derived from B16/BL6 cells (Alexa-B16/BL6). As shown in Fig. 2, the DCs treated with antigens or the DCs treated with antigens and either BLs or ultrasound had fluorescence intensity profiles similar to those of untreated DCs. Flow cytometry confirmed this resemblance, with the percentages of Alexa-B16/BL6-positive cells (M2 gated) determined as 5.7% (antigen only), 6.5% (antigen and BLs), and 7.3% (antigen and ultrasound). In contrast, DCs treated with the combination of all three factors (antigens, BLs, and ultrasound) had an elevated fluorescence intensity profile compared with the other groups. Flow cytometry revealed that the percentage of Alexa-B16/BL6-positive cells was 74.1%.

3.3. Reduction in B16/BL6 lung metastasis following immunization with treated DCs

We employed an *in vivo* B16/BL6 experimental lung metastasis model to determine the anti-metastasis efficacy of DCs treated with tumor antigens delivered using BLs and ultrasound. C57BL/6 mice were immunized twice with bone marrow-derived DCs that were either untreated (no antigen exposure) or into which antigens had been delivered by one of four regimens (antigen alone; antigen + BLs; antigen + ultrasound; or antigen + BLs + ultrasound). As shown in Fig. 3(a), immunization with DCs that had been exposed to no antigen, antigen alone, or antigen with BLs *or* ultrasound weakly suppressed tumor metastasis. In contrast, immunization with DCs that had been exposed to antigens delivered via BLs *and* ultrasound reduced lung metastases four-fold, a decrease that was statistically significant ($P<0.05$) compared to the other groups. These numbers were consistent with the results of macroscopic inspection of lungs from the mice by stereoscopic microscopy, as shown in Fig. 3(b).

4. Discussion

The combination of ultrasound and microbubbles/nanobubbles has been reported to be an effective non-viral gene delivery method

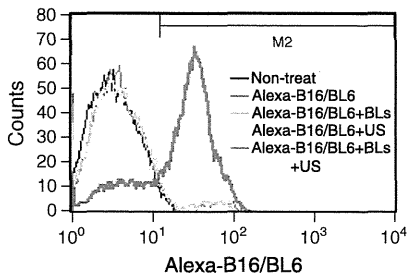

Fig. 2. Intracellular Alexa-B16/BL6 delivery into DCs using BLs and ultrasound. DCs were incubated with Alexa-labeled B16/BL6 extract, exposed (as indicated) to ultrasound and/or BLs, and washed with PBS. Delivery efficiency of Alexa-B16/BL6 was analyzed using flow cytometry. Endocytosis by the DCs was inhibited by the inclusion of 10 mM sodium azide in all solutions and washes. The percentages of M2 gated cell were quantified as follows: Alexa-B16/BL6: 5.7%; Alexa-B16/BL6 + BLs: 6.5%; Alexa-B16/BL6 + ultrasound 7.3%; Alexa-B16/BL6 + BLs + ultrasound: 74.1%.

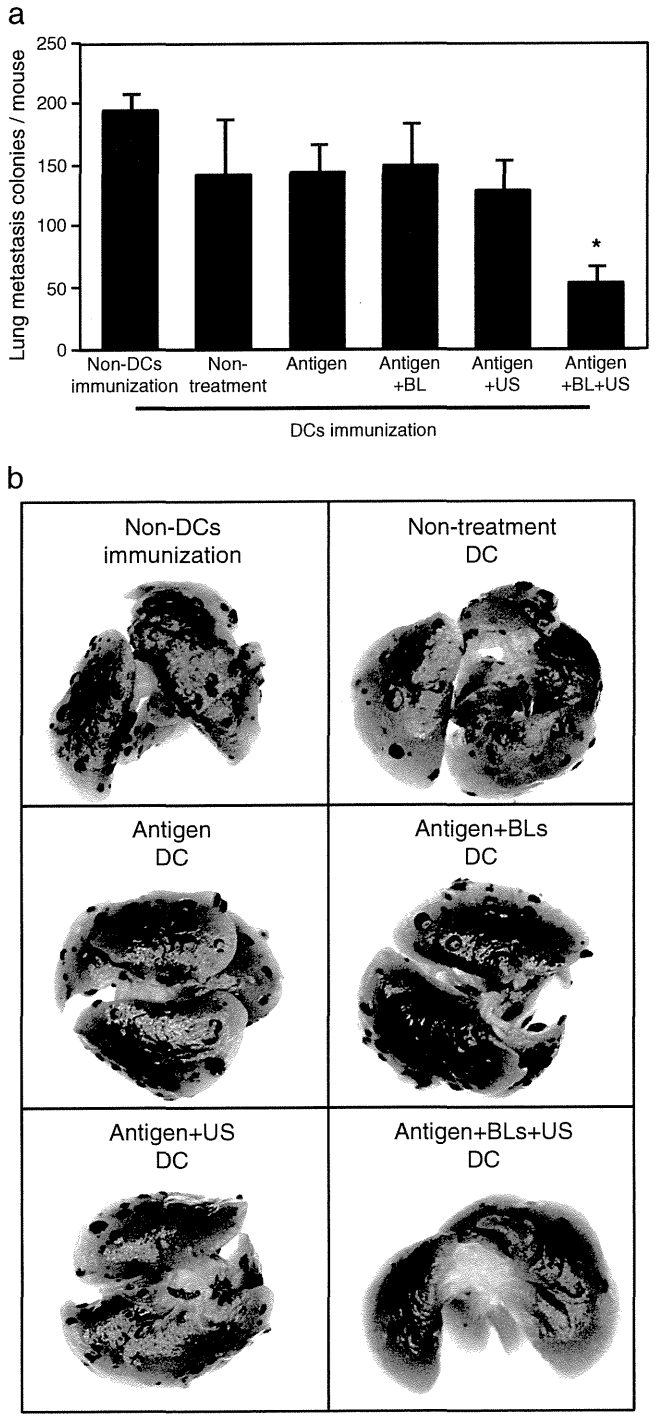

Fig. 3. Reduction of B16/BL6 lung metastasis following immunization with B16/BL6-treated DCs. DCs were treated with B16/BL6-extracted antigens and cultured as described in Materials and methods. C57BL/6 mice were immunized with the DCs twice with a one-week interval. One week after the second immunization, B16/BL6 cells were injected into the tail vein; after another two weeks, animals were sacrificed and lungs assessed for metastases. (a) Counts of lung metastatic colonies (means ± SDs; n = 6). *P < 0.05 (ANOVA, comparing all DC-immunized groups). (b) Images of lung by stereomicroscope.

for whole cells. This technique also has been applied for peptide and protein delivery [38–40]. In a previous study, we proposed the use of this technique for the delivery of novel antigens into DCs for cancer immunotherapy [29]. Entry into cells is believed to reflect the presence of transient pores in the cell membrane, permitting extracellular molecules direct access to the cytosol [21,28,41]. The present study confirmed that antigen was delivered into DCs by the combination of BLs and ultrasound, with delivery observed despite inhibition of the endocytic pathway. Thus, BLs appear to play a role similar to that of microbubbles for ultrasound-mediated substrate delivery. The present study also demonstrated an inverse correlation between the size of the substrate (MW of FITC-dextran) and the efficiency of delivery (fluorescence intensity). These results are consistent with a dependence of antigen delivery on pore size, which in turn depends on the degree of sonoporated cell membranes by BLs. The effect of pore size is expected to limit the delivery of larger molecules. However, this effect should not prevent the application of BL/ultrasound methods for antigen delivery, given that we were able to demonstrate the immunotherapeutic potential of the technique in an *in vivo* mouse model of lung cancer metastasis. As shown in the present work, we still observed delivery (albeit at a reduced level) even for a molecule (FITC-dextran) with a MW of 70,000. FITC-dextran is a bulky polymer with a straight chain; by comparison, most proteins are tightly packed, with a resulting decrease in apparent size. Therefore, various antigens of a range of sizes should still be able to be delivered into DCs using the BL/ultrasound delivery system.

Melanoma is generally considered a highly immunogenic cancer, and several melanoma-associated antigens (e.g., MAGE, MART-1, gp-100) have been identified [8,42]. However, we thought that it was important to establish an antigen delivery system that was suitable for various extracts containing unknown TAAs, since such a technique would be applicable for the induction of a variety of CTL clones [6]. In the present study, we tested BL/ultrasound delivery with TAAs obtained (via butanol extraction) from B16/BL6 cells. The use of butanol extraction is especially appealing because this method has been shown to solubilize a subset of hydrophobic proteins [33] that would presumably include various known and novel TAAs. Antigens delivered to the cytosol of DCs are expected to induce MHC class I presentation by these DCs, in turn inducing antigen-specific CTLs [12]. In the present work, the utility of BL/ultrasound delivery of a crude extract was demonstrated for the B16/BL6 antigens both *in vitro* (Fig. 2) and *in vivo* (Fig. 3).

The *in vivo* assay described here tested the efficacy of B16/BL6 antigens in reducing lung metastasis. Specifically, DCs were exposed to antigens in the presence of BLs and ultrasound, and the treated cells were used for prophylactic immunization of mice. Immunization significantly decreased lung metastasis, indicating that the treated DCs induced a B16/BL6-specific anti-tumor immune response. Given the poor prognosis seen with metastases [3,4], and the challenge of preventing systemic metastasis in the long term, such a therapeutic strategy for metastatic cancer is desperately needed. From this perspective, DC-based cancer immunotherapy is an attractive option: this approach should induce systemic and specific immune responses via antigen presentation, and while also controlling metastasis and recurrence in the longer term via immunological memory [6]. Matheoud et al. reported that immunization of DCs has a potency to reduce the metastasis in therapeutic model (by post-immunization) [43]. To induce more effective immune responses, we are optimizing about antigen delivery for DCs by BLs/ultrasound. After optimization, we will attempt to prevent metastasis in therapeutic model. The combination of BLs and ultrasound is expected to induce effective immune response in DC-based cancer immunotherapy by delivering various TAAs into DCs for potential clinical applications.

Acknowledgments

The authors thank Mr. Eisuke Namai, Mr. Yasuyuki Shiono, Mr. Ken Osawa, Ms. Motoka Kawamura, Mr. Ryo Tanakadate, Mr. Kunihiko Matsuo, Mr. Yudai Kawashima, Mr. Hitoshi Uruga, and Ms. Mutsumi Seki (Teikyo University) for their technical assistance,

and Mr. Yasuhiko Hayakawa and Mr. Kosho Suzuki (Nepa Gene Co., Ltd.) for their technical advice regarding ultrasound exposure. This study was supported by the Program for Promotion of Fundamental Studies in Health Sciences of the National Institute of Biomedical Innovation (NIBIO). This work was supported by JSPS KAKENHI (20240053 and 23300192) and Health and Labour Science Research Grants from Ministry of Health, Labour and Welfare.

References

[1] J.W. Gamel, S.L. George, M.J. Edwards, H.F. Seigler, The long-term clinical course of patients with cutaneous melanoma, Cancer 95 (2002) 1286–1293.
[2] C.M. Balch, S.J. Soong, M.B. Atkins, A.C. Buzaid, A. Houghton Jr., J.M. Kirkwood, K.M. McMasters, M.F. Mihm, D.L. Morton, D.S. Reintgen, M.I. Ross, A. Sober, J.A. Thompson, J.F. Thompson, An evidence-based staging system for cutaneous melanoma, CA Cancer J. Clin. 54 (2004) 131–149.
[3] C. Garbe, P. Terheyden, U. Keiholz, O. Kolbl, A. Hauschild, Treatment of melanoma, Dtsch. Arztebl. Int. 105 (2008) 845–851.
[4] U. Vaishampayan, J. Abrams, D. Darrah, V. Jones, M.S. Mitchell, Active immunotherapy of metastatic melanoma with allogeneic melanoma lysates and interferon, Clin. Cancer Res. 3696 (2002) 3696–3701.
[5] E.M. Levy, M.P. Roberti, J. Mordoh, Natural kiiller cells in human cancer: from biological functions to clinical applications, J. Biomed. Biotechnol. 2011 (2011) 676198.
[6] K. Palucka, H. Ueno, J. Banchereau, Recent developments in cancer vaccines, J. Immunol. 186 (2011) 1325–1331.
[7] P.W. Kantoff, C.S. Higano, N.D. Shore, E.R. Berger, E.J. Small, D.F. Penson, C.H. Redfern, A.C. Ferrari, R. Dreicer, R.B. Sims, Y. Xu, M.W. Frohlich, P.F. Schellhammer, Sipuleucel-T immunotherapy for castration-resistant prostate cancer, N. Engl. J. Med. 363 (2010) 411–422.
[8] S.A. Rosenberg, J.C. Yang, P.F. Robbins, J.R. Wunderlich, P. Hwu, R.M. Sherry, D.J. Schwartzentruber, S.L. Topalian, N.P. Restifo, A. Filie, R. Chang, M.E. Dudley, Cell transfer therapy for cancer: lessons from sequential treatment of a patient with metastatic melanoma, J. Immunother. 26 (2003) 385–393.
[9] P.W. Kantoff, T.J. Schuetz, B.A. Blumenstein, L.M. Glode, D.L. Bilhartz, M. Wyand, K. Manson, D.L. Panicali, R. Laus, J. Schlom, W.L. Dahut, P.M. Arlen, J.L. Gulley, W.R. Godfrey, Overall survival analysis of a phase II randomized controlled trial of a poxviral based PSA-targeted immunotherapy in metastatic castration-resistant prostate cancer, J. Clin. Oncol. 28 (2010) 1099–1105.
[10] F.O. Nestle, A. Farkas, C. Conrad, Dendritic-cell-based therapeutic vaccination against cancer, Curr. Opin. Immunol. 17 (2005) 163–169.
[11] J. Copier, A. Dalgleish, Overview of tumor cell-based vaccines, Int. Rev. Immunol. 25 (2006) 297–319.
[12] R.N. Germain, MHC-dependent antigen processing and peptide presentation: providing ligands for T lymphocyte activation, Cell 76 (1994) 287–299.
[13] P.A. Antony, C.A. Piccirillo, A. Akpinarli, S.E. Finkelstein, P.J. Speiss, D.R. Surman, D.C. Palmer, C.C. Chan, C.A. Klebanoff, W.W. Overwijk, S.A. Rosenberg, N.P. Restifo, CD8+ T cell immunity against a tumor/self-antigen is augmented by CD4+ T helper cells and hindered by naturally occurring T regulatory cells, J. Immunol. 174 (2005) 2591–2601.
[14] P. Elamanchili, M. Diwan, M. Cao, J. Samuel, Characterization of poly(D, L-lactic-co-glycolic acid) based nanoparticulate system for enhanced delivery of antigens to dendritic cells, Vaccine 22 (2004) 2406–2412.
[15] N. Okada, T. Saito, K. Mori, Y. Masunaga, Y. Fujii, J. Fujita, K. Fujimoto, T. Nakanishi, K. Tanaka, S. Nakagawa, T. Mayumi, T. Fujita, A. Yamamoto, Effects of lipofectin-antigen complexes on major histocompatibility complex class I-restricted antigen presentation pathway in murine dendritic cells and on dendritic cell maturation, Biochem. Biophys. Acta 1527 (2001) 97–101.
[16] K. Kawamura, N. Kadowaki, R. Suzuki, S. Udagawa, S. Kasaoka, N. Utoguchi, T. Kitawaki, N. Sugimoto, N. Okada, K. Maruyama, T. Uchiyama, Dendritic cells that endocytosed antigen-containing IgG-liposomes elicit effective antitumor immunity, J. Immunother. 29 (2006) 165–174.
[17] T. Yoshikawa, N. Okada, A. Oda, K. Matsuo, K. Matsuo, Y. Mukai, Y. Yoshioka, T. Akagi, M. Akashi, S. Nakagawa, Development of amphiphilic gamma-PGA-nanoparticle based tumor vaccine: potential of the nanoparticulate cytosolic protein delivery carrier, Biochem. Biophys. Res. Commun. 366 (2008) 408–413.
[18] L. Wang, H. Ikeda, Y. Ikuta, M. Schmitt, Y. Miyahara, Y. Takahashi, X. Gu, Y. Nagata, Y. Sasaki, K. Akiyoshi, J. Sunamoto, H. Nakamura, K. Kuribayashi, H. Shiku, Bone marrow-derived dendritic cells incorporate and process hydrophobized poly-saccaride/oncoprotein complex as antigen presenting cells, Int. J. Oncol. 14 (1999) 695–701.
[19] P. Machy, K. Serre, L. Leserman, Class I-restricted presentation of exogenous antigen acquired by Fcgammareceptor-mediated endocytosis is regulated in dendritic cells, Eur. J. Immunol. 30 (2000) 848–857.
[20] W.J. Greenleaf, M.E. Bolander, G. Sarkar, M.B. Goldring, J.F. Greenleaf, Artificial cavitation nuclei significantly enhance acoustically induced cell transfection, Ultrasound Med. Biol. 24 (1998) 587–595.
[21] Y. Taniyama, K. Tachibana, K. Hiraoka, M. Aoki, S. Yamamoto, K. Matsumoto, T. Nakamura, T. Ogihara, Y. Kaneda, R. Morishita, Development of safe and efficient novel nonviral gene transfer using ultrasound: enhancement of transfection efficiency of naked plasmid DNA in skeletal muscle, Gene Ther. 9 (2002) 372–380.
[22] S. Chen, J.H. Ding, R. Bekeredjian, B.Z. Yang, R.V. Shohet, S.A. Johnston, H.E. Hohmeier, C.B. Newgard, P.A. Grayburn, Efficient gene delivery to pancreatic islets with ultrasonic microbubble destruction technology, Proc. Natl. Acad. Sci. U. S. A. 103 (2006) 8469–8474.
[23] A. Aoi, Y. Watanabe, S. Mori, M. Takahashi, G. Vassaux, T. Kodama, Herpes simplex virus thymidine kinase-mediated suicide gene therapy using nano/microbubbles and ultrasound, Ultrasound Med. Biol. 34 (2008) 425–434.
[24] Z.P. Shen, A.A. Brayman, L. Chen, C.H. Miao, Ultrasound with microbubbles enhances gene expression of plasmid DNA in the liver via intraportal delivery, Gene Ther. 15 (2008) 1147–1155.
[25] S. Sonoda, K. Tachibana, E. Uchino, A. Okubo, M. Yamamoto, K. Sakoda, T. Hisatomi, K.H. Sonoda, Y. Negishi, Y. Izumi, S. Takao, T. Sakamoto, Gene transfer to corneal epithelium and keratocytes mediated by ultrasound with microbubbles, Investig. Ophthalmol. Vis. Sci. 47 (2006) 558–564.
[26] K. Iwanaga, K. Tominaga, K. Yamamoto, M. Habu, H. Maeda, S. Akifusa, T. Tsujisawa, T. Okinaga, J. Fukuda, T. Nishihara, Local delivery system of cytotoxic agents to tumors by focused sonoporation, Cancer Gene Ther. 14 (2007) 354–363.
[27] Y. Taniyama, K. Tachibana, K. Hiraoka, T. Namba, K. Yamasaki, N. Hashiya, M. Aoki, T. Ogihara, K. Yasufumi, R. Morishita, Local delivery of plasmid DNA into rat carotid artery using ultrasound, Circulation 105 (2002) 1233–1239.
[28] R. Suzuki, Y. Oda, N. Utoguchi, K. Maruyama, Progress in the development of ultrasound-mediated gene delivery systems utilizing nano- and microbubbles, J. Control. Release 149 (2011) 36–41.
[29] R. Suzuki, Y. Oda, N. Utoguchi, E. Namai, Y. Taira, N. Okada, N. Kadowaki, T. Kodama, K. Tachibana, K. Maruyama, A novel strategy utilizing ultrasound for antigen delivery in dendritic cell-based cancer immunotherapy, J. Control. Release 133 (2009) 198–205.
[30] K. Inaba, M. Inaba, M. Deguchi, K. Hagi, R. Yasumitsu, S. Ikehara, S. Muramatsu, R.M. Steinman, Granulocytes, macrophages, and dendritic cells arise from a common major histocompatibility complex class II-negative progenitor in mouse bone marrow, Proc. Natl. Acad. Sci. U. S. A. 90 (1993) 3038–3042.
[31] R. Suzuki, T. Takizawa, Y. Negishi, K. Hagisawa, K. Tanaka, K. Tanaka, K. Sawamura, N. Utoguchi, T. Nishioka, K. Maruyama, Gene delivery by the combination of novel liposomal bubbles with perfluoropropane and ultrasound, J. Control. Release 117 (2007) 130–136.
[32] R. Suzuki, T. Takizawa, Y. Negishi, N. Utoguchi, K. Sawamura, K. Tanaka, E. Namai, Y. Oda, Y. Matsumura, K. Maruyama, Tumor specific ultrasound enhanced gene transfer in vivo with novel liposomal bubbles, J. Control. Release 125 (2008) 137–144.
[33] N. Labateya, D.M.P. Thomson, M. Durko, G. Shenouda, L. Robb, R. Scanzano, Extraction of human organ-specific cancer neoantigens from cancer cell and plasma membranes with 1-butanol, Cancer Res. 47 (1987) 1058–1064.
[34] I.A. Ignatovich, E.B. Dizhe, A.V. Pavlotskaya, B.N. Akifiev, S.V. Burov, S.V. Orlov, A.P. Perevozchikov, Complexes of plasmid DNA with basic domain 47–57 of the HIV-1 Tat protein are transferred to mammalian cells by endocytosis-mediated pathways, J. Biol. Chem. 278 (2003) 42625–42636.
[35] K. Sandvig, S. Olsnes, Entry of the toxic proteins abrin, modeccin, ricin, and diphtheria toxin into cells. II. Effect of pH, metabolic inhibitors, and ionophores and evidence for toxin penetration from endocytotic vesicles, J. Biol. Chem. 257 (1982) 7504–7513.
[36] D.A. Zaharoff, J.W. Henshaw, B. Mossop, F. Yuan, Mechanistic analysis of electroporation-induced cellular uptake of macromolecules, Exp. Biol. Med. 233 (2008) 94–105.
[37] J.G. Naglich, M. Jure-Kunkel, E. Gupta, J. Fargnoli, A.J. Henderson, A.C. Lewin, R. Talbott, A. Baxter, J. Bird, R. Savopoulos, R. Wills, R.A. Kramer, P.A. Trail, Inhibition of angiogenesis and metastasis in two murine models by the matrix metalloproteinase inhibitor, BMS-275291, Cancer Res. 61 (2001) 8480–8485.
[38] R. Bekeredjian, S. Chen, P.A. Grayburn, R.V. Shohet, Augmentation of cardiac protein delivery using ultrasound targeted microbubble destruction, Ultrasound Med. Biol. 31 (2005) 687–691.
[39] R. Bekeredjian, H.F. Kuecherer, R.D. Kroll, H.A. Katus, S.E. Hardt, Ultrasound-targeted microbubble destruction augments protein delivery in testes, Urology 69 (2007) 386–389.
[40] M. Kinoshita, K. Hynynen, Intracellular delivery of Bak BH3 peptide by microbubble-enhanced ultrasound, Pharm. Res. 22 (2005) 149–156.
[41] M. Duvshani-Eshet, D. Adam, M. Machluf, The effect of albmin-coated microbubbles in DNA delivery mediated by therapeutic ultrasound, J. Control. Release 112 (2005) 156–166.
[42] P. van der Bruggen, C. Traversari, P. Chomez, C. Lurguin, E. De Plaen, B. Van den Eynde, A. Knuth, T. Boon, A gene encoding an antigen recognized by cytolytic T lymphocytes on a human melanoma, Science 254 (1991) 1643–1647.
[43] D. Matheoud, C. Baey, L. Vimeux, A. Tempez, M. Valente, P. Louche, A.L. Bon, A. Hosmalin, V. Feuillet, Dendritic cells crosspresent antigens from live B16 cells more efficiently than from apoptotic cells and protect from melanoma in a therapeutic model, PLoS One 6 (4) (2011) e19104.

Laboratories of Bio-Functional Molecular Chemistry[1] and Toxicology and Safety Science[2], Graduate School of Pharmaceutical Sciences, Osaka University, Japan

Hepatotoxicity of sub-nanosized platinum particles in mice

Y. YAMAGISHI[1], A. WATARI[1], Y. HAYATA[1], X. LI[1], M. KONDOH[1], Y. TSUTSUMI[2], K. YAGI[1]

Received July 19, 2012, accepted August 30, 2012

Dr. Akihiro Watari, Laboratory of Bio-Functional Molecular Chemistry, Graduate School of Pharmaceutical Sciences, Osaka University, Suita, Osaka 565-0871, Japan
akihiro@phs.osaka-u.ac.jp

Pharmazie 68: 178–182 (2013) *doi: 10.1691/ph.2013.2141*

Nano-sized materials are widely used in consumer products, medical devices and engineered pharmaceuticals. Advances in nanotechnology have resulted in materials smaller than the nanoscale, but the biologic safety of the sub-nanosized materials has not been fully assessed. In this study, we evaluated the toxic effects of sub-nanosized platinum particles (snPt) in the mouse liver. After intravenous administration of snPt (15 mg/kg body weight) into mice, histological analysis revealed acute hepatic injury, and biochemical analysis showed increased levels of serum markers of liver injury and inflammatory cytokines. In contrast, administration of nano-sized platinum particles did not produce these abnormalities. Furthermore, snPt induced cytotoxicity when directly applied to primary hepatocytes. These data suggest that snPt have the potential to induce hepatotoxicity. These findings provide useful information on the further development of sub-nanosized materials.

1. Introduction

Nanotechnology involves manipulation of matter on the scale of the nanometer and has the potential to improve quality of life via functional products. Nanomaterials are commonly defined as objects with dimensions of 1 to 100 nm and are now widely used in electronics, catalysts, clothing, drugs, diagnostic devices, and cosmetics (Baughman et al. 2002; Patra et al. 2010; Service et al. 2007; Ariga et al. 2010). Recent progress in the field has allowed the creation of sub-nanosized materials that have different physicochemical properties, including improved conductivity, durability and strength. Although these materials may be useful for industrial and scientific purposes, the biologic safety of these materials has not been fully evaluated (Nel et al. 2006; Oberdorster et al. 2005).

Nano-sized platinum particles (nPt) are used for industrial applications and in consumer products, such as cosmetics, supplements and food additives (Gehrke et al. 2011; Horie et al. 2011). The biological influence of exposure to nPt has been previously investigated. For example, nPt has anti-oxidative activity (Watanabe et al. 2009; Onizawa et al. 2009; Kajita et al. 2007), and may be useful for the medical treatment of diseases related to oxidative stress and aging. However, some reports suggest that these substances can induce inflammation in mice or impair DNA integrity (Pelka et al. 2009; Park et al. 2010). Thus, the understanding of the biological influences of nPt has still not been definitively established, and our knowledge regarding the biological effects of sub-nanosized platinum particles (snPt) is severely lacking.

Nano-sized particles can enter and penetrate the lungs, intestines and skin. The degree of penetration depends on the size and surface features of the nano-sized particle. Furthermore, nanoparticles can enter the circulatory system and migrate to various organs, such as the brain, spleen, liver, kidney and muscles (Zhu et al. 2008; Furuyama et al. 2009; Oberdorster et al. 2004; Ai et al. 2011). The liver is a vital organ that is involved in the uptake of nutrients and the elimination of waste products and pathogens from the blood; it is also an important organ for the clearance of nanoparticles. However, some nanoparticles are hepatotoxic (Nishimori et al. 2009a, b; Ji et al. 2009; Cho et al. 2009; Folkmann et al. 2009). In the present study, we investigated the influence of sub-nanosized platinum particles (snPt) on the liver.

2. Investigations and results

To investigate the acute liver toxicity of snPt, we administered snPt (15 mg/kg body weight) into mice by intravenous injection. Histological analysis revealed acute hepatic injury, including vacuole degeneration (Fig. 1). Furthermore, administration of snPt at doses over 15 mg/kg resulted in significant elevation of serum alanine aminotransferase (ALT) and aspartate aminotransferase (AST) levels (Fig. 2A and B) and of interleukin-6 (IL-6) levels (Fig. 2C). ALT and AST levels were increased at 3 h to 24 h after intravenous administration at 20 mg/kg snPt (Fig. 3A and B). Cell viability assessment by WST assay demonstrated that direct treatment of isolated hepatocytes with snPt at concentrations of 0.1, 1, 10, 50 and 100 μg/ml resulted in a dose-dependent decrease in hepatocyte viability when compared with vehicle-treated cells (Fig. 4). These observations suggest that snPt induced inflammation and hepatocyte death.

Previous reports showed that biological influences of nanomaterials vary according to material size (Nishimori et al. 2009a, b; Jiang et al. 2008; Oberdorster et al. 2010). Therefore, we examined whether nPt, with a diameter of approximately 15 nm, leads

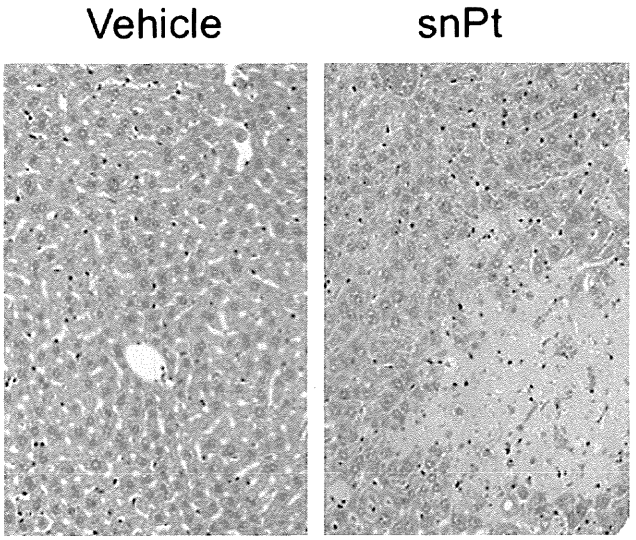

Fig. 1: Histological analysis of liver tissues in snPt-treated mice. snPt was intravenously administered to mice at 15 mg/kg. At 24 h after administration, livers were collected and fixed with 4% paraformaldehyde. Tissue sections were stained with hematoxylin and eosin and observed under a microscope. The pictures show representative data from at least four mice

to a different biologic effect than snPt. As shown in Fig. 5, snPt administration resulted in dose-dependent increases in serum ALT and AST levels, whereas nPt did not. Furthermore, IL-6 levels did not change in response to administration of nPt. These results suggest that the biological effects of platinum particles are dependent on their size.

3. Discussion

The influence of size and of physiochemical properties of nanoparticles on their biologic safety is an important issue. Animal experiments have demonstrated rapid translocation of nanoparticles from the entry site to various organs (Almeida et al. 2011). In particular, nanoparticles tend to concentrate in the liver and are cleared from the body in the feces and urine after intravenous infusion (Ai et al. 2011). While the liver plays a pivotal role in the clearance of nanoparticles, some nanomaterials can induce liver injury. Therefore, we assessed the influence of snPt on the liver and demonstrated that snPt induced liver toxicity *in vitro* and *in vivo*.

Some studies have reported that nPt exert anti-oxidant and anti-inflammatory effects (Watanabe et al. 2009; Onizawa et al. 2009; Kajita et al. 2007), while other studies reported that nPt have negative biological effects. For example, treatment of a human colon carcinoma cell line with nPt resulted in a decrease in cellular glutathione level and impairment in DNA integrity (Pelka et al. 2009). Furthermore, Park et al. (2010) found that nPt prepared from K_2PtCl_6 may induce an inflammatory response in mice. In this study, we found that snPt damaged liver tissues and induced inflammatory cytokines. Kupffer cells present in liver sinusoids may mediate this process via phagocytosis of the particles and subsequent release of inflammatory cytokines. However, when we added snPt to primary hepatocytes, the viability of the cells was significantly reduced, suggesting that snPt may also exert a direct hepatotoxic effect. Thus, the cellular influences of Pt nano- and sub-nano particles may be dependent on the target cells as well as on the size and physical and chemical properties of the particles.

snPt may damage other tissues as well. Cisplatin, a first-line chemotherapy for most cancers, is a platinating agent that can cause kidney damage (Daugaard et al. 1990; Brabec et al. 2005). Furthermore, snPt-induced increases in systemic IL-6 may cause damage to various organs. Further analysis of the distribution and toxic effects of snPt is necessary.

Widespread application of sub-nanosized materials comes with an increased risk of human exposure and environmental release, and the future of nanotechnology will depend on the public acceptance of the risk-benefit ratio. The present study demonstrated that snPt induces hepatotoxicity *in vitro* and *in vivo*. However, our research also indicates that the toxicity of platinum particles could be reduced by altering their size. Additionally, biocompatible coatings can reduce the negative effects of nanoparticles on cells (Oberdorster et al. 2010; Nabeshi et al. 2011; Singh et al. 2007; Clift et al. 2008). Therefore, future studies will contribute to the development of sub-nanosized materials and will also help produce safer products.

4. Experimental

4.1. Materials

Platinum particles with a diameter of 15 nm (nPt) and less than 1 nm (snPt) were purchased from Polytech & Net GmbH (Rostock, Germany). The

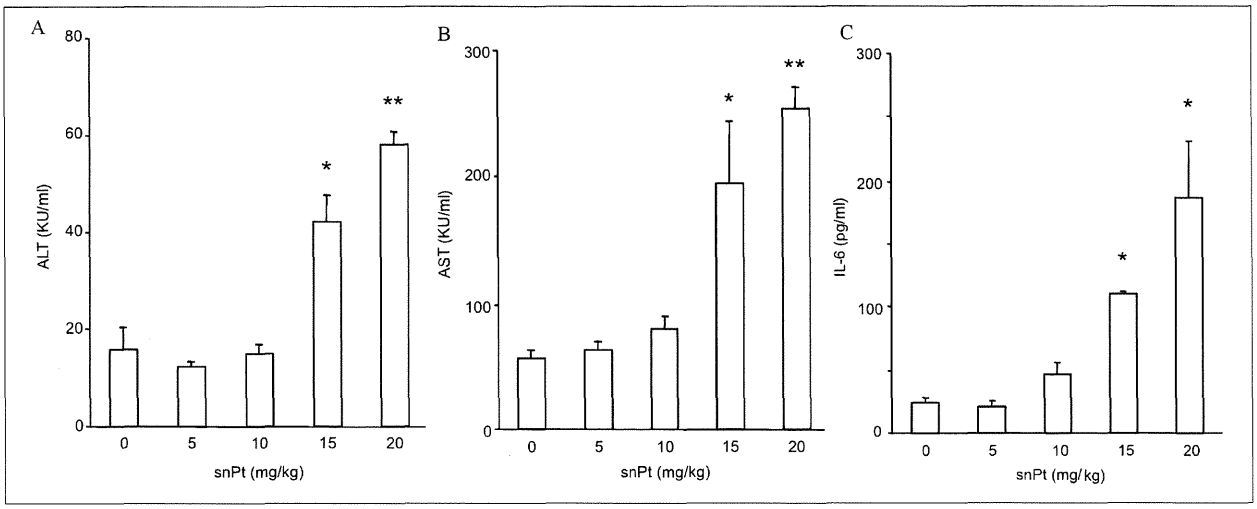

Fig. 2: Dose dependency of snPt-induced liver injury. snPt was intravenously administrated at 5, 10, 15 and 20 mg/kg. At 24 h after administration, blood was recovered, and the resultant serum was used for measurement of ALT (A), AST (B) and IL-6 (C), as described in the "Experimental" section. Data are means ± SEM (n = 3). *Significant difference when compared with the vehicle-treated group (*, $p < 0.05$, **, $p < 0.01$)

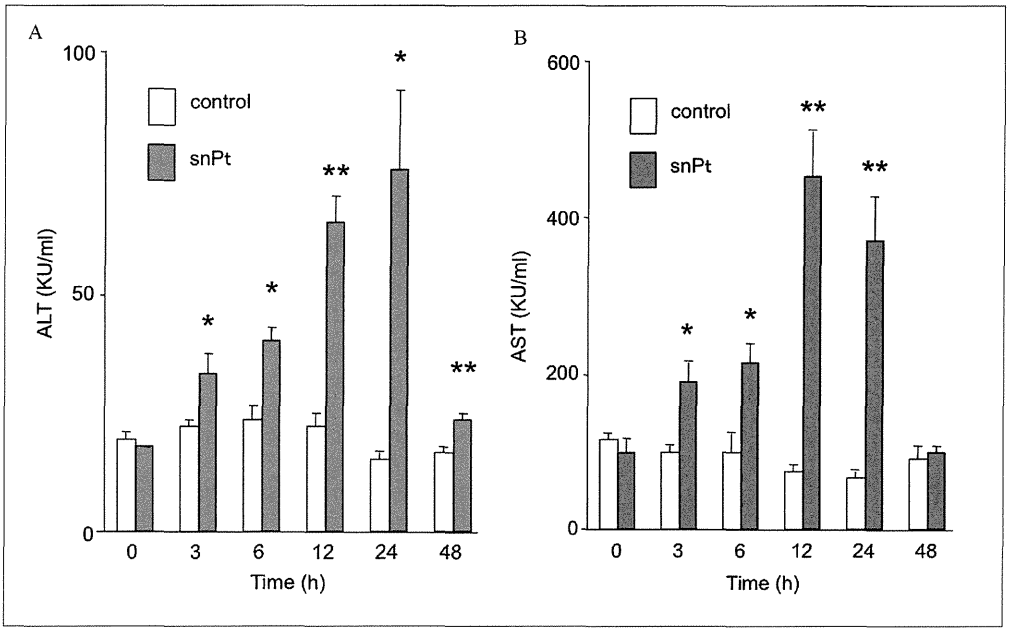

Fig. 3: Time-dependent changes of a biological marker of liver injury. snPt was intravenously administered to mice at 15 mg/kg. Blood was recovered at 3, 6, 12, 24 and 48 h after administration. The serum was used for measurement of ALT (A) and AST (B), as described in the "Experimental" section. Data are means ± SEM (n = 3). *Significant difference when compared with the vehicle-treated group (*, $p < 0.05$, **, $p < 0.01$)

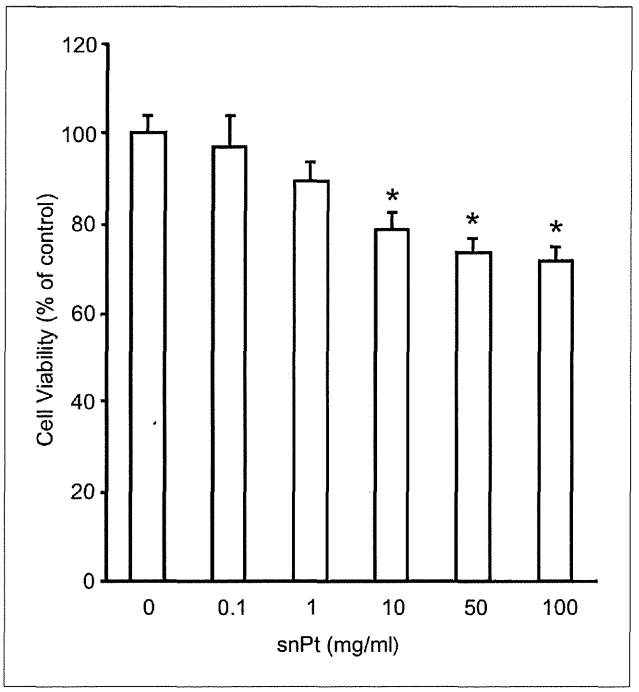

Fig. 4: Cytotoxicity of snPt in hepatic cells. Primary hepatocytes were treated with snPt at 0.1, 1, 10, 50 or 100 μg/ml. After 24 h of culture, cell viability was evaluated with the WST assay, as described in the "Experimental" section. Data are means ± SEM (n = 3). *Significant difference when compared with the vehicle-treated group ($P < 0.05$)

particles were stocked in a 5 mg/ml aqueous suspension. The stock solutions were suspended using a vortex mixer before use. Reagents used in this study were of research grade.

4.2. Animals

BALB/c male mice (8 weeks old) were obtained from Shimizu Laboratory Supplies Co., Ltd. (Kyoto, Japan), and were housed in an environmentally controlled room at 23 ± 1.5 °C with a 12 h light/12 h dark cycle. Mice had access to water and commercial chow (Type MF, Oriental Yeast, Tokyo, Japan). Mice were intravenously injected with nPt or snPt at 5 to 20 mg/kg body weight. The experimental protocols conformed to the ethical guidelines of the Graduate School of Pharmaceutical Sciences, Osaka University.

4.3. Cells

Mouse primary hepatocytes were isolated from BALB/c mice (Shimizu Laboratory Supplies Co.) by the collagenase-perfusion method (Seglen 1976). Isolated hepatocytes were suspended in Williams' E medium containing 10% fetal calf serum, 1 nM insulin, and 1 nM dexamethasone. Next, cell viability was assessed by Trypan blue dye exclusion. Cells that were at least 90% viable were used in this study. Cells were cultured in a humidified 5% CO_2 incubator at 37 °C.

4.4. Histological analysis

After intravenous administration of snPt, mouse livers were removed and fixed with 4% paraformaldehyde. Thin tissue sections were stained with hematoxylin and eosin for histological observation.

4.5. Biochemical assay

Serum alanine aminotransferase (ALT) and aspartate aminotransferase (AST) were measured using commercially available kits (WAKO Pure Chemical, Osaka, Japan), respectively. Interleukin-6 (IL-6) levels were measured with an ELISA kit (BioSource International, Camarillo, CA, USA). These assays were performed according to the manufacturer's protocols.

4.6. Cell viability assay

Cell viability was determined using WST-8 (Nacalai Tesque, Osaka, Japan), according to the manufacturer's protocol. Briefly, 1×10^4 cells/well were seeded on a 96 well plate at 37 °C overnight. After 24 h of treatment with snPt, WST-8 reagent was added to each well. The plate was incubated for 1 h at 37 °C and assessed at an absorbance of 450 nm by a plate reader. Obtained data were normalized to the control group, which was designated as 100%.

4.7. Statistical analysis

Data are presented as means ± SD. Statistical analysis was performed by student's t-test. $P < 0.05$ was considered statistically significant.

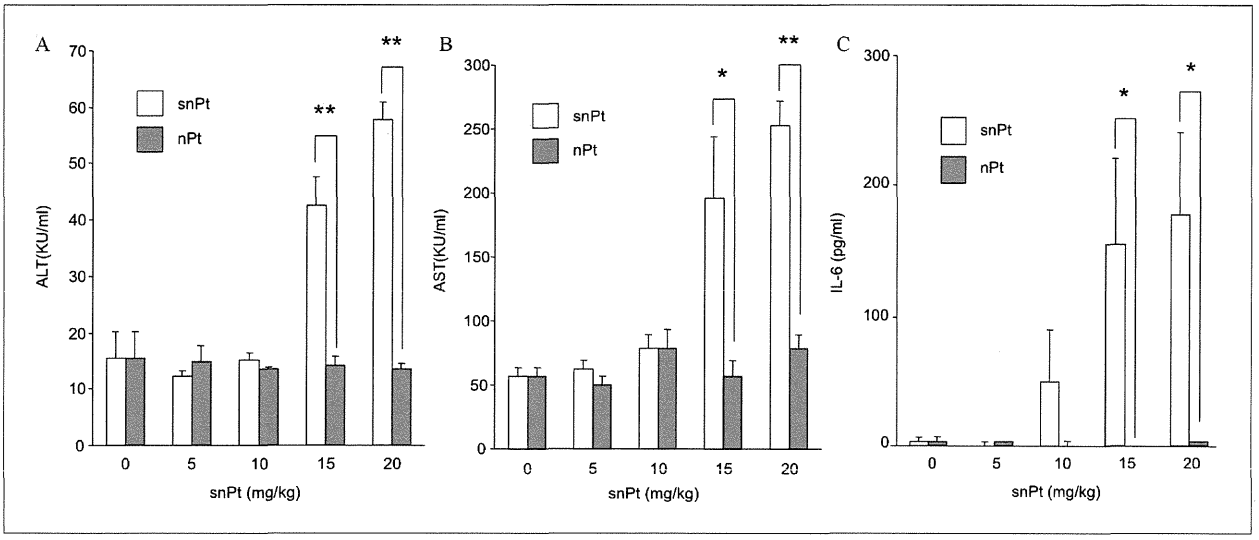

Fig. 5: Effect of particle size of platinum on liver injury. snPt or nPt was intravenously injected into mice at the indicated doses. Blood was recovered at 24 h after injection. Serum ALT (A), AST (B) and IL-6 (C) levels were measured. Data are means ± SEM (n = 3). *Significant difference between the snPt- and nPt-treated groups (*, $p < 0.05$, **, $p < 0.01$)

Acknowledgements: The authors thank all members of our laboratory for useful comments. This study was partly supported by a grant from the Ministry of Health, Labour, and Welfare of Japan.

References

Ai J, Biazar E, Jafarpour M, Montazeri M, Majdi A, Aminifard S, Zafari M, Akbari HR, Rad HG (2011) Nanotoxicology and nanoparticle safety in biomedical designs. Int J Nanomed 6: 1117–1127.

Almeida JP, Chen AL, Foster A, Drezek R (2011) *In vivo* biodistribution of nanoparticles. Nanomedicine (Lond) 6: 815–835.

Ariga K, Hu X, Mandal S, Hill JP (2010) By what means should nanoscaled materials be constructed: molecule, medium, or human? Nanoscale 2: 198–214.

Baughman RH, Zakhidov AA, de Heer WA (2002) Carbon nanotubes–the route toward applications. Science 297: 787–792.

Brabec V, Kasparkova J (2005) Modifications of DNA by platinum complexes. Relation to resistance of tumors to platinum antitumor drugs. Drug Resist Updat 8: 131–146.

Cho WS, Cho M, Jeong J, Choi M, Cho HY, Han BS, Kim HO, Lim YT, Chung BH, Jeong J (2009) Acute toxicity and pharmacokinetics of 13 nm-sized PEG-coated gold nanoparticles. Toxicol Appl Pharmacol 236: 16–24.

Clift MJ, Rothen-Rutishauser B, Brown DM, Duffin R, Donaldson K, Proudfoot L, Guy K, Stone V (2008) The impact of different nanoparticle surface chemistry and size on uptake and toxicity in a murine macrophage cell line. Toxicol Appl Pharmacol 232: 418–427.

Daugaard G (1990) Cisplatin nephrotoxicity: experimental and clinical studies. Dan Med Bull 37: 1–12.

Folkmann JK, Risom L, Jacobsen NR, Wallin H, Loft S, Moller P (2009) Oxidatively damaged DNA in rats exposed by oral gavage to C60 fullerenes and single-walled carbon nanotubes. Environ Health Perspect 117: 703–708.

Furuyama A, Kanno S, Kobayashi T, Hirano S (2009) Extrapulmonary translocation of intratracheally instilled fine and ultrafine particles via direct and alveolar macrophage-associated routes. Arch Toxicol 83: 429–437.

Gehrke H, Pelka J, Hartinger CG, Blank H, Bleimund F, Schneider R, Gerthsen D, Brase S, Crone M, Turk M, Marko D (2011) Platinum nanoparticles and their cellular uptake and DNA platination at non-cytotoxic concentrations. Arch Toxicol 85: 799–812.

Horie M, Kato H, Endoh S, Fujita K, Nishio K, Komaba LK, Fukui H, Nakamura A, Miyauchi A, Nakazato T, Kinugasa S, Yoshida Y, Hagihara Y, Morimoto Y, Iwahashi H (2011) Evaluation of cellular influences of platinum nanoparticles by stable medium dispersion. Metallomics 3: 1244–1252.

Ji Z, Zhang D, Li L, Shen X, Deng X, Dong L, Wu M, Liu Y (2009) The hepatotoxicity of multi-walled carbon nanotubes in mice. Nanotechnology 20: 445101.

Jiang J, Oberdorster G, Elder A, Gelein R, Mercer P, Biswas P (2008) Does Nanoparticle Activity Depend upon Size and Crystal Phase? Nanotoxicology 2: 33–42.

Kajita M, Hikosaka K, Iitsuka M, Kanayama A, Toshima N, Miyamoto Y (2007) Platinum nanoparticle is a useful scavenger of superoxide anion and hydrogen peroxide. Free Radic Res 41: 615–626.

Nabeshi H, Yoshikawa T, Arimori A, Yoshida T, Tochigi S, Hirai T, Akase T, Nagano K, Abe Y, Kamada H, Tsunoda S, Itoh N, Yoshioka Y, Tsutsumi Y (2011) Effect of surface properties of silica nanoparticles on their cytotoxicity and cellular distribution in murine macrophages. Nanoscale Res Lett 6: 93.

Nel A, Xia T, Madler L, Li N (2006) Toxic potential of materials at the nanolevel. Science 311: 622–627.

Nishimori H, Kondoh M, Isoda K, Tsunoda S, Tsutsumi Y, Yagi K (2009) Histological analysis of 70-nm silica particles-induced chronic toxicity in mice. Eur J Pharm Biopharm 72: 626–629.

Nishimori H, Kondoh M, Isoda K, Tsunoda S, Tsutsumi Y, Yagi K (2009) Silica nanoparticles as hepatotoxicants. Eur J Pharm Biopharm 72: 496–501.

Oberdorster G (2010) Safety assessment for nanotechnology and nanomedicine: concepts of nanotoxicology. J Intern Med 267: 89–105.

Oberdorster G, Oberdorster E, Oberdorster J. Nanotoxicology: an emerging discipline evolving from studies of ultrafine particles (2005) Environ Health Perspect 113: 823–839.

Oberdorster G, Sharp Z, Atudorei V, Elder A, Gelein R, Kreyling W, Cox C (2004) Translocation of inhaled ultrafine particles to the brain. Inhal Toxicol 16: 437–445.

Onizawa S, Aoshiba K, Kajita M, Miyamoto Y, Nagai A (2009) Platinum nanoparticle antioxidants inhibit pulmonary inflammation in mice exposed to cigarette smoke. Pulm Pharmacol Ther 22: 340–349.

Park EJ, Kim H, Kim Y, Park K (2010) Intratracheal instillation of platinum nanoparticles may induce inflammatory responses in mice. Arch Pharm Res 33: 727–735.

Patra CR, Bhattacharya R, Mukhopadhyay D, Mukherjee P (2010) Fabrication of gold nanoparticles for targeted therapy in pancreatic cancer. Adv Drug Deliv Rev 62: 346–361.

Pelka J, Gehrke H, Esselen M, Turk M, Crone M, Brase S, Muller T, Blank H, Send W, Zibat V, Brenner P, Schneider R, Gerthsen D, Marko D (2009) Cellular uptake of platinum nanoparticles in human colon carcinoma cells and their impact on cellular redox systems and DNA integrity. Chem Res Toxicol 22: 649–659.

Seglen PO (1976) Preparation of isolated rat liver cells. Methods Cell Biol 13: 29–83.

Service RF. U.S. nanotechnology (2007) Health and safety research slated for sizable gains. Science 315: 926.

Singh S, Shi T, Duffin R, Albrecht C, van Berlo D, Hohr D, Fubini B, Martra G, Fenoglio I, Borm PJ, Schins RP (2007) Endocytosis, oxidative stress and IL-8 expression in human lung epithelial cells upon treatment with fine and ultrafine TiO2: role of the specific surface area and of surface methylation of the particles. Toxicol Appl Pharmacol 222: 141–151.

Watanabe A, Kajita M, Kim J, Kanayama A, Takahashi K, Mashino T, Miyamoto Y (2009) *In vitro* free radical scavenging activity of platinum nanoparticles. Nanotechnology 20: 455105.

Zhu MT, Feng WY, Wang B, Wang TC, Gu YQ, Wang M, Wang Y, Ouyang H, Zhao YL, Chai ZF (2008) Comparative study of pulmonary responses to nano- and submicron-sized ferric oxide in rats. Toxicology 247: 102–111.

A Baculoviral Display System to Assay Viral Entry

Manami Iida,[a,#] Takeshi Yoshida,[a,#] Akihiro Watari,[a] Kiyohito Yagi,[a] Takao Hamakubo,[b] and Masuo Kondoh*,[a]

[a] *Laboratory of Bio-Functional Molecular Chemistry, Graduate School of Pharmaceutical Sciences, Osaka University; Suita, Osaka 565–0871, Japan: and* [b] *Department of Quantitative Biology and Medicine, Research Center for Advanced Science and Technology, The University of Tokyo; Tokyo 153–8904, Japan.*

Received August 9, 2013; accepted August 22, 2013

In this study, we evaluated a baculoviral display system for analysis of viral entry by using a recombinant adenovirus (Ad) carrying a luciferase gene and budded baculovirus (BV) that displays the adenoviral receptor, coxsackievirus and adenovirus receptor (CAR). CAR-expressing B16 cells (B16-CAR cells) were infected with luciferase-expressing Ad vector in the presence of BV that expressed or lacked CAR (CAR-BV and mock-BV, respectively). Treatment with mock-BV even at doses as high as 5 μg/mL failed to attenuate the luciferase activity of B16-CAR cells. In contrast, treatment with CAR-BV with doses as low as 0.5 μg/mL significantly decreased the luciferase activity of infected cells, which reached 65% reduction at 5 μg/mL. These findings suggest that a receptor-displaying BV system could be used to evaluate viral infection.

Key words baculovirus; virus; infection; receptor

The process of viral infection involves entry of the virus into the cell, followed by replication of the viral genome and other viral components in the host cell.[1] Whereas the molecular mechanisms underlying viral replication have largely been elucidated, the key molecules for entry, the viral receptors on host cells, have never been fully identified. Most host receptors are integral membrane proteins, and it is difficult to prepare their recombinant proteins because of their hydrophobicity. Since recombinant proteins are needed to screen inhibitors for viral entry and to produce antibodies against host receptors, preparation of inhibitors, such as chemicals, peptides and antibodies, for viral entry has been delayed.

The baculoviral expression system in insect cells has been widely used for preparation of recombinant proteins.[2] Hamakubo and colleagues found that baculoviral particles are released from baculovirus-infected cells; the membranes of these budded baculovirus (BV) display host-cell-derived membrane proteins.[3] Interestingly, the activity and topology of these host-origin proteins remain intact in the baculoviral membrane.[4] Moreover, a baculoviral envelope protein gp64 trasngenic mice were generated, and method to generate monoclonal antibodies against membrane proteins by immunization of gp64 transgenic mice with membrane protein-displayed baculovirus has been established.[5] These findings suggest that a baculoviral display system may be useful for assaying viral entry, leading to creation of monoclonal antibodies against host receptors.

In the present study, we investigated whether a baculoviral display system work as an assay system for viral entry using recombinant adenovirus (Ad) vector and a receptor for Ad, coxsackievirus and adenovirus receptor (CAR).[6]

MATERIALS AND METHODS

Cell Culture Mouse melanoma B16-CAR cells[7] were cultured in Dulbecco's modified Eagle's medium (DMEM) supplemented with 10% fetal calf serum (FCS) and 2 mg/mL G418. 293 cells were cultured in DMEM supplemented with 10% FCS. Sf9 cells (Invitrogen, Gaithersburg, MD, U.S.A.) were cultured in Grace's insect cell culture medium supplemented with 10% FCS.

Preparation of Recombinant Ad Vector An improved *in vitro* ligation method[8] was used to generate a recombinant type 5 Ad vector that encoded a fusion protein comprising enhanced green fluorescence protein and firefly luciferase (EGFPLuc). The recombinant Ad vector (Ad-EGFPLuc) was purified from transfected cells by using $CsCl_2$ gradient centrifugation. Viral titers were determined spectrophotometrically.[9]

Preparation of Recombinant Baculoviruses Recombinant BVs were prepared by using the Bac-to-Bac Baculovirus Expression System (Invitrogen) according to the manufacturer's protocol. Sf9 cells were transduced with the CAR-encoding bacmid, recombinant CAR-BV were recovered by centrifugation of the conditioned medium,[10] and Sf9 cells were infected with recombinant CAR-BV. At 72 h after infection, the culture supernatant of the infected Sf9 cells was centrifuged to pellet recombinant CAR-BV, which were resuspended in Tris-buffered saline and stored at 4°C until use.

Western Blotting Mock-BV, CAR-BV, and B16-CAR cells were lysed in lysis buffer (25 mM Tris–HCl [pH 7.5], 1% Triton X-100, 0.5% sodium deoxycholate, 150 mM NaCl, 5 mM ethylenediaminetetraacetic acid (EDTA)) containing protease inhibitors (Sigma, St. Louis, MO, U.S.A.). The protein content of the resulting lysates was measured by using the BCA protein assay kit (Pierce Chemical, Rockford, IL, U.S.A.), with bovine serum albumin as the standard. Samples of cellular lysates (20 μg) and BV lysates (5 μg) underwent sodium dodecyl sulfate–polyacrylamide gel electrophoresis followed by blotting of proteins to a polyvinylidene difluoride membrane. The membrane was treated with 5% skim milk to inhibit nonspecific binding, incubated with an anti-goat CAR antibody (R&D Systems, Minneapolis, MN, U.S.A.), and then incubated with a peroxidase-labeled secondary antibody. Immunoreactive bands were visualized by using chemiluminescence reagents (GE Healthcare, Buckinghamshire, U.K.).

Infection Assay Aliquots of Ad-EGFPLuc vector (4×10^7

The authors declare no conflict of interest.

[#] These authors contributed equally to this work.

* To whom correspondence should be addressed. e-mail: masuo@phs.osaka-u.ac.jp

viral particles per mL) were incubated with mock-BV or CAR-BV (0.5 or 5 μg/mL) and an anti-BV gp64 antibody (0.065 or 0.65 μg/mL; AcV1, Santa Cruz Biotechnology, CA, U.S.A.) for 2 h at 37°C to prevent non-specific binding of gp64 to cells. B16-CAR cells were seeded onto 96-well plates (2×10^4 cells per well); 50 μL of the mixture of Ad vector and BVs was added to each well and incubated for 15 min, after which the medium was replaced with fresh growth medium. After an additional 24 h of culture, the luciferase activity in the lysates was measured by using a luminometer.

Statistical Analysis The data were analyzed for statistical significance by Student's *t*-test.

RESULTS AND DISCUSSION

First, we prepared CAR-displaying BV. Lysates of CAR-B16 cells, a mouse myeloma line that expresses mouse CAR, yielded two bands, at 40 and 46 kDa (Fig. 1). In contrast, lysates of CAR-BV showed not only the 40-kDa form but also several bands lower and upper than 40 kDa (Fig. 1); these bands likely represent post-translational modifications. CAR contains two *N*-glycosylation sites and two disulfide-bonded loops in the extracellular domain. The putative molecular sizes of CAR are 40 and 46 kDa, in its non-glycosylated form and glycosylated forms, respectively.[6] Protein folding and post-translational processing, particularly *N*-glycosylation, in insect cells differs markedly from that in mammal cells.[11–13] For example, prolactin receptor expressed in insect cells was 29 kDa larger than that expressed in mammalian cells; this difference was attributed to *N*-glycosylation and ubiquitination.[14]

To investigate whether CAR-BV inhibited adenoviral entry, B16-CAR cells were infected with Ad vector expressing luciferase in the presence of mock-BV or CAR-BV. Whereas treatment with mock-BV at doses as high as 5 μg/mL did not attenuate the luciferase activity of the infected B16-CAR cells, treatment with as little as 0.5 μg/mL CAR-BV significantly decreased their luciferase activity, which reaching 65% reduction at 5 μg/mL (Fig. 2). These findings indicate that CAR-BV prevented the infection of cells by Ad vector. In support of our finding, recombinant prolactin receptor expressed in insect cells and prolactin receptor purified from rabbit mammary gland showed similar specificity and affinity to prolactin.[14] Accordingly, the post-translational modification of CAR in insect cells may not hamper the ability of Ad vector to bind to its receptor.

Our current findings suggest that a baculoviral display system may be useful in the analysis of viral infection, which involves binding of the viral envelope to the viral receptor in the membrane of the host cell. Baculoviral display systems have also been used widely to generate monoclonal antibodies against the extracellular regions of membrane proteins.[3,15] Future applications of baculoviral display systems might contribute the analysis of the mechanisms underlying the entry of pathogens into host cells and the generation of inhibitors of viral entry.

Acknowledgments We thank Prof. H. Mizuguchi (Osaka University) and the members of our laboratory for providing us CAR cDNA and CAR-expressing B16 cells, and useful comments, respectively. This work was supported by a Grant-in-Aid for Scientific Research from the Ministry of Education, Culture, Sports, Science and Technology of Japan (24390042), by a Health and Labour Sciences Research Grant from the Ministry of Health, Labor, and Welfare of Japan, the Takeda Science Foundation and the Nakatomi Foundation.

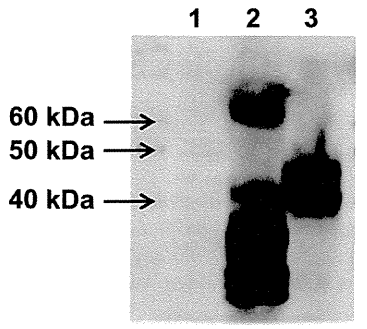

Fig. 1. Preparation of CAR-Displaying BV

Lysates of mock-BV (5 μg, lane 1), CAR-BV (5 μg, lane 2), and CAR-B16 cells (20 μg, lane 3) underwent Western blotting by using a polyclonal goat anti-CAR antibody and a peroxidase-labeled secondary antibody. The arrows indicate the positions of marker proteins.

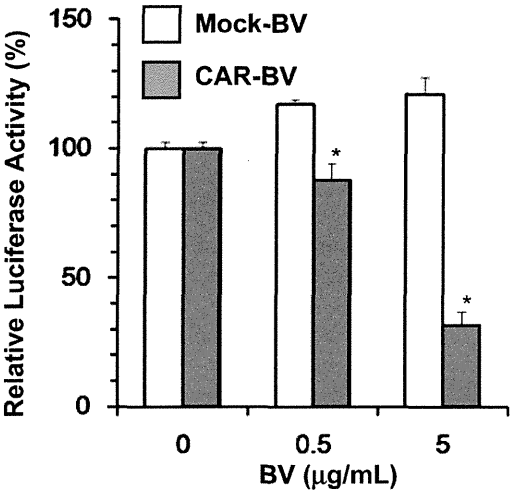

Fig. 2. Effects of CAR-Displaying BV on Ad Vector Infection

Ad vectors (4×10^7 viral particles per mL) were incubated with mock-BV or CAR-BV at 0, 0.5, or 5 μg/mL for 2 h at 37°C. B16-CAR cells were exposed to the Ad–BV mixtures, cultured for 24 h in fresh medium, lysed, and evaluated for luciferase activity. Data are given as luciferase activity relative to that of cells not exposed to BV. Data are shown as mean±S.D. (n=3). *Significant difference compared with mock-BV ($p<0.05$).

REFERENCES

1) Cosset FL, Lavillette D. Cell entry of enveloped viruses. *Adv. Genet.*, **73**, 121–183 (2011).
2) Bieniossek C, Imasaki T, Takagi Y, Berger I. MultiBac: expanding the research toolbox for multiprotein complexes. *Trends Biochem. Sci.*, **37**, 49–57 (2012).
3) Tanaka T, Takeno T, Watanabe Y, Uchiyama Y, Murakami T, Yamashita H, Suzuki A, Aoi R, Iwanari H, Jiang SY, Naito M, Tachibana K, Doi T, Shulman AI, Mangelsdorf DJ, Reiter R, Auwerx J, Hamakubo T, Kodama T. The generation of monoclonal antibodies against human peroxisome proliferator-activated receptors (PPARs). *J. Atheroscler. Thromb.*, **9**, 233–242 (2002).
4) Sakihama T, Masuda K, Sato T, Doi T, Kodama T, Hamakubo T. Functional reconstitution of G-protein-coupled receptor-mediated adenylyl cyclase activation by a baculoviral co-display system. *J.*

Biotechnol., **135**, 28–33 (2008).
5) Saitoh R, Ohtomo T, Yamada Y, Kodama N, Nezu J, Kimura N, Funahashi S, Furugaki K, Yoshino T, Kawase Y, Kato A, Ueda O, Jishage K, Suzuki M, Fukuda R, Arai M, Iwanari H, Takahashi K, Sakihama T, Ohizumi I, Kodama T, Tsuchiya M, Hamakubo T. Viral envelope protein gp64 transgenic mouse facilitates the generation of monoclonal antibodies against exogenous membrane proteins displayed on baculovirus. *J. Immunol. Methods*, **322**, 104–117 (2007).
6) Arnberg N. Adenovirus receptors: implications for targeting of viral vectors. *Trends Pharmacol. Sci.*, **33**, 442–448 (2012).
7) Yamashita M, Ino A, Kawabata K, Sakurai F, Mizuguchi H. Expression of coxsackie and adenovirus receptor reduces the lung metastatic potential of murine tumor cells. *Int. J. Cancer*, **121**, 1690–1696 (2007).
8) Mizuguchi H, Kay MA. A simple method for constructing E1- and E1/E4-deleted recombinant adenoviral vectors. *Hum. Gene Ther.*, **10**, 2013–2017 (1999).
9) Maizel JV Jr, White DO, Scharff MD. The polypeptides of adenovirus. I. Evidence for multiple protein components in the virion and a comparison of types 2, 7A, and 12. *Virology*, **36**, 115–125 (1968).
10) Saeki R, Kondoh M, Kakutani H, Tsunoda S, Mochizuki Y, Hamakubo T, Tsutsumi Y, Horiguchi Y, Yagi K. A novel tumor-targeted therapy using a claudin-4-targeting molecule. *Mol. Pharmacol.*, **76**, 918–926 (2009).
11) Altmann F, Staudacher E, Wilson IB, Marz L. Insect cells as hosts for the expression of recombinant glycoproteins. *Glycoconj. J.*, **16**, 109–123 (1999).
12) Voss T, Ergulen E, Ahorn H, Kubelka V, Sugiyama K, Maurer-Fogy I, Glossl J. Expression of human interferon omega 1 in Sf9 cells. No evidence for complex-type *N*-linked glycosylation or sialylation. *Eur. J. Biochem.*, **217**, 913–919 (1993).
13) Yeh JC, Seals JR, Murphy CI, van Halbeek H, Cummings RD. Site-specific *N*-glycosylation and oligosaccharide structures of recombinant HIV-1 gp120 derived from a baculovirus expression system. *Biochemistry*, **32**, 11087–11099 (1993).
14) Cahoreau C, Petridou B, Cerutti M, Djiane J, Devauchelle G. Expression of the full-length rabbit prolactin receptor and its specific domains in baculovirus infected insect cells. *Biochimie*, **74**, 1053–1065 (1992).
15) Hayashi I, Takatori S, Urano Y, Miyake Y, Takagi J, Sakata-Yanagimoto M, Iwanari H, Osawa S, Morohashi Y, Li T, Wong PC, Chiba S, Kodama T, Hamakubo T, Tomita T, Iwatsubo T. Neutralization of the gamma-secretase activity by monoclonal antibody against extracellular domain of nicastrin. *Oncogene*, **31**, 787–798 (2012).

Journal of
PERIODONTAL RESEARCH

J Periodont Res 2013

JOURNAL OF PERIODONTAL RESEARCH
doi:10.1111/jre.12119

Gene delivery to periodontal tissue using Bubble liposomes and ultrasound

M. Sugano[1,2], Y. Negishi[2], Y. Endo-Takahashi[2], N. Hamano[2], M. Usui[3], R. Suzuki[4], K. Maruyama[4], Y. Aramaki[2], M. Yamamoto[1]

[1]Department of Periodontology, Showa University School of Dentistry, Tokyo, Japan, [2]Department of Drug Delivery and Molecular Biopharmaceutics, School of Pharmacy, Tokyo University of Pharmacy and Life Sciences, Tokyo, Japan, [3]Division of Periodontology, Kyushu Dental University, Kokurakita-ku, Kitakyushu City, Japan and [4]Laboratory of Drug and Gene Delivery, Faculty of Pharma-Sciences, Teikyo University, Tokyo,Japan

Sugano M, Negishi Y, Endo-Takahashi Y, Hamano N, Usui M, Suzuki R, Maruyama K, Aramaki Y, Yamamoto M. Gene delivery to periodontal tissue using Bubble liposomes and ultrasound. J Periodont Res 2013; doi: 10.1111/jre.12119. © 2013 John Wiley & Sons A/S. Published by John Wiley & Sons Ltd

Background and Objective: Periodontitis is the most common inflammatory disease caused by oral biofilm infection. For efficient periodontal treatment, it is important to enhance the outcome of existing regenerative therapies. The physical action of an ultrasound may be able to deliver a therapeutic gene or drugs into the local area of the periodontium being treated for periodontal regeneration. Previously, we developed "Bubble liposomes" as a useful carrier for gene or drug delivery, and reported that delivery efficiency was increased with high-frequency ultrasound *in vitro* and *in vivo*. Hence, the aim of the present study was to examine the possibility of delivering genes into gingival tissues using Bubble liposomes and ultrasound.

Material and Methods: We attempted to deliver naked plasmid DNA encoding luciferase or enhanced green fluorescent protein (EGFP) into the lower labial gingiva of Wistar rats using Bubble liposomes, with or without ultrasound exposure. Ultrasound parameters were optimized for intensity (0-4.0 W/cm^2) and exposure time (0–120 s) to establish the most efficient conditions for exposure. The efficacy and duration of gene expression in the gingiva were investigated using a luciferase assay and fluorescence microscopy.

Results: The strongest relative luciferase activity was observed when rats were treated under the following ultrasound conditions: 2.0 W/cm^2 intensity and 30 s of exposure time. Relative luciferase activity, 1 d after gene delivery, was significantly higher in gingiva treated using Bubble liposomes and ultrasound than in gingiva of the other treatment groups. Histological analysis also showed that distinct EGFP-expressing cells were observed in transfected gingiva when rats were treated under optimized conditions.

Conclusion: From these results, the combination of Bubble liposomes and ultrasound provides an efficient technique for delivering plasmid DNA into the gingiva. This technique can be applied for the delivery of a variety of therapeutic molecules into target tissue, and may serve as a useful treatment strategy for periodontitis.

Yoichi Negishi, PhD, Department of Drug Delivery and Molecular Biopharmaceutics, School of Pharmacy, Tokyo University of Pharmacy and Life Sciences 1432-1 Horinouchi, Hachioji, Tokyo 192-0392 Japan
Tel: +81 42 676 3183
Fax: +81 42 676 3182
e-mail: negishi@toyaku.ac.jp

Key words: Bubble liposomes; gene delivery; periodontitis; ultrasound

Accepted for publication June 06, 2013

Periodontitis is the most common oral inflammatory disease. The pathogenic factor is a biofilm, also called dental plaque, which is composed of periodontal bacteria. Dental biofilms, particularly in deep periodontal pockets, cause inflammatory destruction of periodontal tissues, resulting in alveolar bone absorption and tooth loss. Two main strategies for periodontal therapy exist: infection control and periodontal regeneration. Periodontitis

is regarded as a local infection because it is an inflammatory disease mainly caused by dental biofilms. Therefore, the majority of conventional treatments aim to remove the biofilm on the local periodontium. For example, a local drug-delivery system is positioned as an adjunctive therapy in nonsurgical periodontal management, and some antibiotics have been orally administered to combat bacteria located in periodontal pockets. In order to maintain an effective concentration of tetracycline, the controlled release of tetracycline paste into the deep pockets of patients with periodontitis has been reported (1). However, an efficient periodontal antibiotic-delivery system that exhibits clinical therapeutic effectiveness has yet to be established.

On the other hand, periodontal regenerative therapy is regarded as an effective method of stimulating and guiding proliferating periodontal stem cells in the surrounding periodontal tissue. A large number of clinical studies have shown significant bone fill or clinical attachment level gain when an enamel matrix derivative, guided tissue-regeneration membranes and/or bone grafts were used for treatment of bone defects (2,3). However, there are also limitations in the indication of periodontal regenerative therapy and it is difficult to regenerate lost periodontal tissues. The development of more efficient periodontal therapy based on a new concept is needed, and an absolute treatment strategy may be established by utilizing a method that promotes the effects of existing treatments.

The latest developments reported have shown that gene delivery has the potential to promote wound healing or reduce healing complications that prevent regeneration (4,5). If wound healing in the local periodontium can be promoted during periodontal regeneration, it may lead to rapid recovery. Gene delivery into periodontal tissues may contribute to the up-regulation of neovascularization and cell proliferation, which are important factors for sufficient regeneration. However, technical limitations in *in-vivo* studies, including release control, stability, safety and/or convenience, still need to be overcome. Recently, the use of ultrasound (US), as physical energy to enhance the permeability of mucosa or skin, has been reported (6,7). In addition, the effects of US can be applied to enhance the delivery of therapeutic molecules, such as genes, drugs or peptides, into target tissues. The mechanism of gene delivery with US exposure is "cavitation", which generates many microbubbles and then results in their destruction. The efficiency of cavitation is enhanced by combining US with synthetic microbubbles such as Optison (8,9), Albunex (10) or Sonazoid (11). Previously, we developed "Bubble liposomes (BL)" as a novel gene-delivery carrier and reported that the combination of BL and high-frequency US was an effective gene-delivery method *in vitro* and *in vivo* (12–14). We postulate that when BL are exposed to US, they are destroyed, thereby generating a jet stream by cavitation, and consequently transient pores appear in the membranes of cells, through which extracellular plasmid DNA can enter the cytosol.

The development of gene delivery using US technology may contribute to further advancements in the efficiency and optimization of existing periodontal treatments. Few studies have described gene delivery to periodontal tissues, and the development of periodontal gene therapy may provide a new treatment strategy in the future. Therefore, we investigated whether it was possible to deliver genes to the gingiva, which is a typical periodontal tissue and the site of periodontal inflammation, by our transfection system using BL and US.

Material and methods

Animals

Seven-week-old male Wistar rats (Tokyo Laboratory Animals Science, Tokyo, Japan) were used for all animal experiments. All studies were approved by the Animal Experiment Committee of Tokyo University of Pharmacy and Life Sciences. Rats were given feed and tap water *ad libitum* throughout the experimental period.

Preparation of BL

BL were prepared using a previously described method (12,13). In brief, polyethylene glycol liposomes, composed of 1,2-dipalmitoyl-*sn*-glycero-3-phosphocholine (DPPC) (NOF Corporation, Tokyo, Japan) and 1,2-distearoyl-*sn*-glycero-3-phosphatidylethanolamine-polyethyleneglycol (DSPE-PEG_{2000}-OMe) (NOF Corporation), at a molar ratio of 94 : 6, were prepared using a reverse-phase evaporation method. All reagents were dissolved in chloroform/diisopropyl ether (1 : 1; vol/vol). Phosphate-buffered saline was added to the lipid solution, and the mixture was sonicated and then evaporated at 47°C. Then, the organic solvent was completely removed, and the size of the liposomes was adjusted to less than 200 nm using extruding equipment and a sizing filter (pore size = 200 nm) (Nuclepore Track-Etch Membrane, Whatman plc, Maidstone, UK). Lipid concentrations were measured using the Phospholipids C test (Wako Pure Chemical Industries Ltd., Osaka, Japan), and BL were prepared from liposomes and perfluoropropane gas (Takachio Chemical Ind. Co. Ltd., Tokyo, Japan). First, 2-mL sterilized vials containing 0.8 mL of a liposome suspension (lipid concentration = 1 mg/mL) were filled with perfluoropropane gas, capped and then pressurized with a further 3 mL of perfluoropropane gas. The vial was placed in a bath-type sonicator (42 kHz, 100 W) (BRANSONIC 2510j-DTH; Branson Ultrasonics Co., Danbury, CT, USA) for 5 min to form BL.

Plasmid DNA

Two reporter plasmids were used in this study. The pcDNA3-Luc plasmid, which is derived from pGL3-basic (Promega, Madison, WI, USA), is an expression vector that encodes the firefly luciferase gene under the control of the cytomegalovirus promoter. The pCAG-EGFP plasmid (provided by NEPA GENE, Co. Ltd., Chiba, Japan) is an expression vector encoding enhanced green fluorescent protein (EGFP) under the control of the CAG promoter. The CAG promoter is a

hybrid promoter of cytomegalovirus enhancer element and chicken beta-actin promoter, and is frequently used to drive high levels of gene expression in mammalian expression vectors.

In-vivo gene delivery using BL and US

Wistar rats were anesthetized with 40 mg/mL of pentobarbital throughout each procedure via intra-abdominal injection. The limbs and head of each rat were fixed on an original flat board, and the labial gingiva was clearly exposed for the gene-transfection procedure by eversion of the lower lip. A 10-μL mixture of pDNA (10 μg) and BL (5 μg) was injected into the labial gingiva of the incisor in the lower jaw using a 33-gauge syringe (HAMILTON COMPANY, Reno, NV, USA) and US was immediately applied to the injection site. A Sonitron 2000 (NEPA GENE, Co. Ltd) was used as an ultrasound generator, which had a US probe of 6 mm in diameter. US conditions were as follows: frequency, 1 MHz; duty, 50%; intensity, 0–4 W/cm^2; time, 0–120 s.

Measurement of luciferase activity

Several days after the injection, the rats were killed by overdose of anesthesia, and the gingival tissue in the US-exposed area was collected and homogenized with a POLYTRON (KINEMATICA, INC., New York, NY, USA). The cell lysate and tissue homogenates were diluted with lysis buffer [0.1 M Tris–HCl (pH 7.8), 0.1% Triton X-100 and 2 mM EDTA]. Luciferase activity was then measured using a luciferase assay system (Promega) and a luminometer (LB96V; Belthold Japan Co. Ltd., Tokyo, Japan). Activity was indicated as relative light units per mg of protein.

Histological observation of EGFP expression and local cell viability

To identify transfected cells, the mandible, including the incisors and surrounding gingival tissues, was dissected 1 d after the gene-delivery procedure. Dental samples were fixed with 4% paraformaldehyde in phosphate-buffered saline, decalcified with 10% EDTA and embedded in optimal cutting temperature compound. Then, 10-μm-thick frozen sections were cut using a cryostat and EGFP-expressing cells were observed using a fluorescence microscope (Axiovert 200M; Carl Zeiss, Tokyo, Japan). In parallel, serial vertical sections in which EGFP expression was observed were also cut, and hematoxylin and eosin staining was carried out. Microscopy (BZ-8100; KEYENCE, Osaka, Japan) of hematoxylin and eosin-stained specimens was used for morphological observations and for assessing tissue damage. Then, the dental samples were stained with NADH tetrazolium reductase to assess cytotoxicity of US-mediated gene delivery. NADH tetrazolium reductase staining was performed as described in a previous study (15). In brief, 8-μm cryosections were prepared then incubated in a solution of Tris–HCl buffer, Nitro blue tetrazolium (NBT) (Wako Pure Chemical Industries Ltd.) and β-NADH (Wako) at 37°C for 60 min. The sections were then immersed in serial acetone solutions at the concentrations 30%, 60%, 90%, 60% and 30%, washed with deionized H_2O, then mounted with aqueous medium.

Statistical analysis

All data are shown as mean ± SD (n = 5). The Mann–Whitney U-test was used to determine the significance of any differences. Differences detected in multiple comparison tests were assessed using a two-way repeated-measures ANOVA. Differences associated with a $p < 0.05$ were considered significant.

Results

We first attempted to deliver naked pDNA into rat gingival tissue using BL and US under the conditions described in our previous study, in which naked pDNA was delivered into the tongue tissue of mice (16). To optimize the US conditions for *in-vivo* gene delivery into gingival tissue, we examined the US intensity and US exposure time. These US parameters represent two factors that decide the efficiency of delivery. US intensity ranged between 0 and 4.0 W/cm^2. Relative luciferase activity was significantly higher in groups treated at a US intensity of 2.0 W/cm^2 than in the group not exposed to US (Fig. 1A). A slight increase in luciferase intensity was also observed at US intensities of 0.5 and 4.0 W/cm^2. We also examined the effect of US exposure time on transfection efficiency. The highest luciferase activity was observed at a US exposure time of 30 s. Delivery efficiency did not increase in a time-dependent manner, and high activity was maintained until 120 s (Fig. 1B).

Next, we examined the duration of gene expression induced after treatment with BL and US exposure. High luciferase activity was observed 1 d after gene transfection. Lower luciferase activity was observed at subsequent time points, and the lowest luciferase activity was observed 7 d after gene delivery (Fig. 2).

From these results, we decided that the optimal US conditions of gene delivery to the gingiva were US intensity of 2.0 W/cm^2 and US exposure time of 30 s. To assess the combined effect of BL and US, rats were treated under these optimized conditions. Significantly higher gene expression was confirmed in the group treated with BL and US exposure than in the group treated with pDNA alone (Fig. 3). Relative luciferase activity in the group treated with pDNA+BL remained as low as that of the pDNA-only group. In contrast, luciferase activity was slightly higher in the pDNA+US group than in the pDNA-only or pDNA+BL groups.

We also attempted to identify transfected cells by analyzing EGFP expression using fluorescence microscopy. The number of EGFP-expressing cells was higher in gingival tissue treated with BL and US than in the other treatment groups (data not shown). The majority of EGFP-expressing cells were concentrated in the vicinity of the midline of the transfected area. Some sporadic cells expressed EGFP in the connective tissue of the gingiva in the other treat-

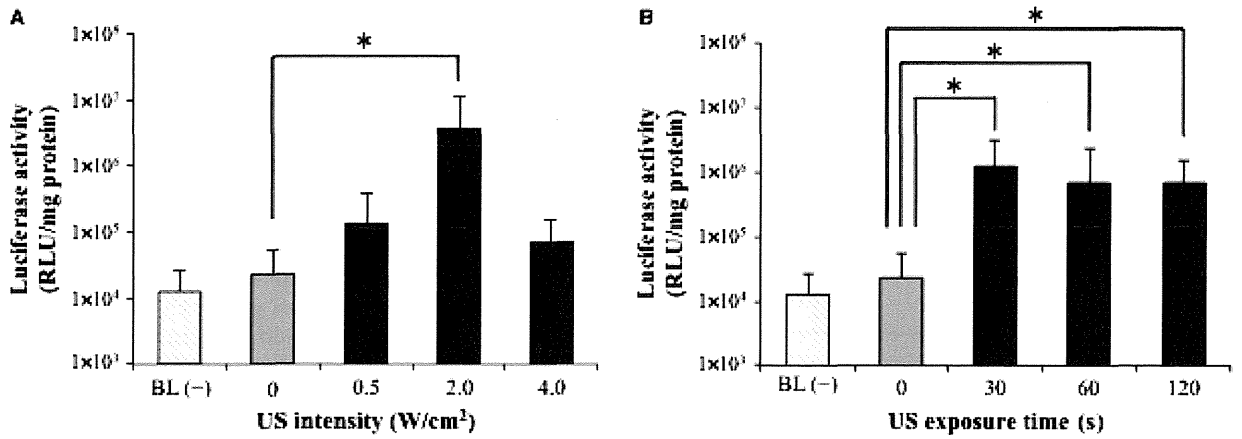

Fig. 1. Characteristics of the ultrasound (US) gene-delivery system using Bubble liposomes (BL). To examine the optimal parameters for BL and US-mediated gene delivery into gingival tissue, rats were subjected to alterations of two US conditions: the US intensity and the US exposure time. The other transfection conditions were as follows: pDNA (pCMV-Luciferase), 10 μg; BL, 5 μg; US frequency, 1 MHz; duty, 50%. Relative luciferase activity activity [measured as relative light units (RLU)] was determined 1 d after transfection. Data are shown as mean ± SD. The BL (-) group was injected with a mixture of pDNA and 5 μl of phosphate-buffered saline instead of with BL. (A) Variations in the gene-expression levels induced by changes in the US intensity. US intensity was set at 0, 0.5, 2.0 or 4.0 W/cm^2. US duration was set at 30 s. *$p < 0.05$, Mann–Whitney *U*-test ($n = 5$), significantly different from 0 W/cm^2 (no US exposure). (B) Variations in the gene-expression levels induced by changes in the US exposure time. US intensity was set at 2.0 W/cm^2. US duration was set at 0, 30, 60 or 120 s. *$p < 0.05$, Mann–Whitney *U*-test ($n = 5$), significantly different from 0 s (no US exposure).

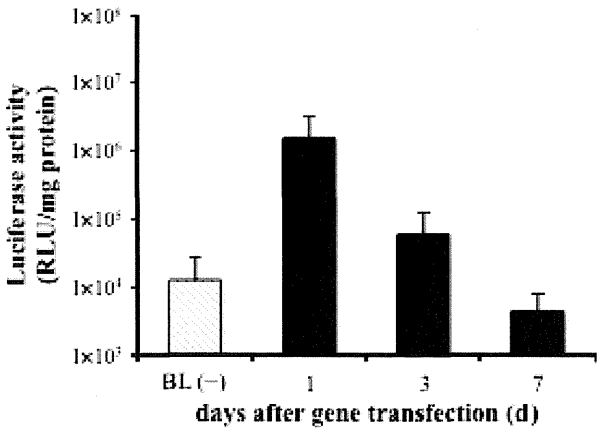

Fig. 2. Duration of gene expression in gingival tissue transfected using Bubble liposomes (BL) and ultrasound (US). Relative luciferase activity [measured as relative light units (RLU)] was examined 1, 3 and 7 d after gene transfection. Transfection conditions were as follows: pDNA (pCMV-Luciferase), 10 μg; BL, 5 μg; and US conditions were: frequency, 1 MHz; duty cycle, 50%; intensity, 2.0 W/cm^2; and time, 30 s. Data are shown as mean ± SD The BL (−) group was injected with a mixture of pDNA and 5 μl of phosphate-buffered saline instead of BL.

ment groups. We further observed the accumulation of many EGFP-expressing cells in both the gingival epithelium layer and the connective tissue layer when a combination of BL and US exposure was used (Fig. 4). Macroscopic observations of US-exposed areas revealed that inflammatory signs such as redness, swelling or hemorrhage were not observed. Furthermore, hematoxylin and eosin-stained samples showing distinct EGFP expression exhibited no inflammation or bleeding. In all delivery areas, including the gingival epithelium and connective tissue, no signs of cytotoxicity, such as inflammatory cell infiltration, were observed (Fig. S1).

Discussion

The prevalence of periodontal disease is increasing, and morbid conditions are becoming complicated. While the onset and progression of periodontitis is greatly affected by dental biofilms, periodontal disease is a multifactorial disease that arises from the relationships among the pathogen (bacterial), the host and the environment. The immunity of periodontal tissue is diminished for genetic effects in some patients. For example, genetic mutations in cytokines, including interleukin-1 and tumor necrosis factor-alpha, have been partially associated with susceptibility to periodontitis (17,18). Moreover, four kinds of genopathy, namely Papillon–Lefèvre syndrome, Haim–Munk syndrome, Chédiak–Higashi syndrome and cyclic neutropenia, have exhibited signs of periodontitis as a result of the dysfunction of a single gene. Therefore, an extensive approach against the individual processes of development and risk factors is required for effective periodontal treatment.

Gene delivery is an innovative approach used to regulate a gene causing a disease and can consequently